Angewandte Chemie
Eine Zeitschrift der Gesellschaft Deutscher Chemiker

Supporting Information

Molecular Electrostatic Potential and Noncovalent Interactions in Derivatives of Group 8 Elements

*Andrea Daolio, Andrea Pizzi, Miriam Calabrese, Giancarlo Terraneo, Simone Bordignon, Antonio Frontera, and Giuseppe Resnati**

anie_202107978_sm_miscellaneous_information.pdf

Table of Contents

S1. Materials and Methods.

S1.1 Classification of σ-hole interactions

Some features of σ-hole interactions are quite similar independent of the group of the Periodic Table to which the electrophilic atom belongs. This is the case for the strength of interactions formed by a given nucleophile with different electrophilic atoms of the same group, this strength increases with the polarizability of the atom and with the electron-withdrawing abilities of the residues bound close to it. Other features vary with the group to which the electrophilic site belongs. For instance, σ-hole interactions are more likely to deviate somewhat from the extension of the σ-covalent bond that generates the σ-hole when the σ-hole is on an atom of groups 15 and 16 than when it is an atom of groups 14 or 17. A systematic terminology which classifies sub-classes of σ-hole interactions as a function of the group of the electrophilic atom offers the advantage to recognize and declare these differences.

S1.2 Details on Materials

All compounds were purchased from commercial suppliers (Sigma-Aldrich, TCI, Matrix Scientific) and used without further purification.

S1.3 Details on Methods

HAZARDS: osmium tetroxide (OsO_4) is very toxic by inhalation, in contact with skin and eyes, or if swallowed. Store it in tightly closed glass containers and in very well ventilated place. OsO_4 can penetrate plastics.[1] The compound is quite volatile (vapor pressure: 7 mmHg, 20 °C) and has to be handled only under well ventilated hoods. In case of contact with eyes or skin, rinse immediately with plenty of water and seek medical advice. If you feel unwell, seek immediately for medical advice.

^{1}H and ^{13}C NMR spectra in solution were recorded at ambient temperature on Nuclear Magnetic Resonance Spectrometer AVANCE III, Bruker-BioSpin (400 MHz). The Larmor frequency for ^{1}H and ^{13}C on those instruments were 400.13 and 100.61 MHz, respectively. All the chemical shifts are given in ppm and the coupling constants in Hz. $CDCl_3$ was used as both solvent and internal standard (as residual $CHCl_3$) in ^{1}H NMR spectra and in ^{13}C. SSNMR spectra were recorded at room temperature using a Jeol ECZR 600 spectrometer operating at 150.91 and 60.81 MHz for ^{13}C and ^{15}N nuclei, respectively. Zirconia rotors (volume 60 μL, diameter 3.2 mm) were filled with sample powders. ^{13}C CPMAS spectra were obtained with a 20 kHz rotation speed, ramp cross-polarization pulse sequence, 3.5 ms contact time, a 2.0 μs ^{1}H pulse at 90°, optimized recycle time of 13.6 s (256 scans) or 15 s (256 scans). ^{15}N CPMAS spectra were obtained with a 12 kHz rotation speed, ramp cross-polarization pulse sequence, 7 ms contact time, a 2.0 μs ^{1}H pulse at 90°, optimized recycle time of 13.6 s (5140 scans) or 15 s (9400 scans). In all spectra the two-pulse phase modulation (TPPM) decoupling scheme was used with a 108.5 kHz radio frequency field. Glycine methylene and glycine signals (δ = 43.7 ppm and δ = 33.4 ppm relative to NH_3) were used as external standards for ^{13}C and ^{15}N chemical shifts. FT-IR spectra for solids were obtained using a Nicolet Nexus FT-IR spectrometer equipped with UATR unit. Solution IR spectra were obtained using a demountable liquid cell kit mounted on the same instrument and equipped with PTFE O-ring and CaF_2 windows (round, 32 mm, Sigma Aldrich).

The single crystal data of the compounds were collected at 100 K using a Bruker SMART APEX II CCD area detector diffractometer. Data collection, unit cell refinement and data reduction were performed using Bruker SAINT. Structures were solved by direct methods using SHELXT[2] and refined by full-matrix least-squares on F^2 with anisotropic displacement parameters for the non-H atoms using SHELXL-2016/6[3]. Absorption correction was performed based on multi-scan procedure using SADABS. Structure analysis was aided by use of the programs PLATON[4]. The hydrogen atoms were calculated in ideal positions with isotropic displacement parameters set to 1.2xUeq of the attached atom.

S2. Synthesis and Characterization.

S2.1 Synthetic Procedures and Basic Characterization

General synthetic procedure

1 mL of a CH_2Cl_2 solution containing 0.11 mmol of osmium tetroxide are added dropwise under stirring to 4 mL of a solution of the Lewis base, containing 0.10 mmol of electron donor site, in the same solvent in a borosilicate glass flask. The resulting colorless solution instantaneously turns to yellow/brown. The solvent is removed over 1~3 hours under a gentle stream of anhydrous nitrogen gas. Brownish crystals, suitable for X-Ray diffraction for adducts **2a**-**c**, are formed on the walls and at the bottom of the flask in nearly quantitative yields. Crystals are collected and characterized.

Synthesis and Characterization of 1a·$(OsO_4)_2$ (cocrystal 2a)

The brown co-crystals of **2a** were synthetized following the general procedure starting from 0.11 mmol of OsO_4 and 0.05 mmol of 4,4'-bipyridine (**1a**), respectively. FTIR (solid, cm^{-1}) 1605, 1409, 1215, 906, 812, 630, 470. ^{1}H NMR (400.13 MHz, $CDCl_3$) δ 8.72 (d, J = 4.6 Hz, 4H), 7.56 (d, J =5.2 Hz, 4H). ^{13}C NMR (100.61 MHz, $CDCl_3$) δ 149.9 (s, N<u>C</u>), 146.1 (s, NCC<u>C</u>), 121.9 (s, NC<u>C</u>).

Synthesis and Characterization of 1b·$(OsO_4)_2$ (cocrystal 2b)

The brown co-crystals of **2b** were synthetized following the general procedure starting from 0.11 mmol of OsO_4 and 0.05 mmol and 1,2-di(pyridin-4-yl)ethane (**1b**). FTIR (solid, cm^{-1}) 1613, 1428, 1201, 902, 829, 539. ^{1}H NMR (400.13 MHz, $CDCl_3$) δ 8.50 (dd, J = 5.4, 1.6 Hz, 4H), 7.07 (d, J = 5.2, 1.6 Hz, 4H), 2.95 (s, 4H). ^{13}C NMR (100.61 MHz, $CDCl_3$) δ 150.2 (s, NCC<u>C</u>), 149.2 (s, N<u>C</u>) 124.2 (s, NC<u>C</u>), 35.7 (s, <u>C</u>H_2).

Synthesis and Characterization of 1c·$(OsO_4)_2$ (cocrystal 2c)

The brown co-crystals of **2c** were synthetized following the general procedure starting from 0.11 mmol of OsO_4 and 0.05 mmol of [4,4'-bipyridine] 1,1'-dioxide polyhydrate (**1c**). FTIR (solid, cm^{-1}) 1470, 1207, 1172, 909, 823, 548. ^{1}H NMR (400.13 MHz, $CDCl_3$) δ 8.28 (dd, J = 5.4, 2.0 Hz, 4H), 7.49 (dd, J = 5.3, 2.0 Hz, 4H). ^{13}C NMR (100.61 MHz, $CDCl_3$) δ 140.1 (s, N<u>C</u>), 133.0 (s, NCC<u>C</u>), 123.1 (s, NC<u>C</u>).
1c·$(H_2O)_2$[5] was prepared through crystallization of **1c** from non-anhydrous CH_2Cl_2. **1c·$(H_2O)_2$** is hygroscopic; on storage in an open flask in the air the water content of the sample increases (as shown byIR and ^{1}H NMR analyses). Different batches were obtained containing 3-6 water molecules per dioxide molecule (**1c·$(H_2O)_n$**, n=3-6). When OsO_4 and different batches of **1c·$(H_2O)_n$** (n=2-6) were crystallized using the general synthetic procedure described above, **1c·$(OsO_4)_2$** was exclusively isolated (yields >85%) as shown by IR (solid and solution), ^{1}H NMR, and single crystal X-ray analyses.

Synthesis and Characterization of 1d·$(OsO_4)_2$ (cocrystal 2d)

The brown powder of co-crystal **2d** was synthetized following the general procedure starting from 0.11 mmol of OsO_4 and 0.05 mmol of 1,3-di(pyridin-4-yl)propane (**1d**). FTIR (solid, cm^{-1}) 1612, 1424, 901, 819, 621, 512. ^{1}H NMR (400.13 MHz, $CDCl_3$) δ 8.41 (*d*, J = 5.6 Hz, 4H), 7.06 (*d*, J = 5.6 Hz, 4H), 2.59 (*t*, J = 8.0 Hz, 4H), 1.92 (*m*, J = 8.0 Hz, 2H). ^{13}C NMR (100.61 MHz, $CDCl_3$) δ 151.3 (NCC<u>C</u>), 143.7 (NC<u>C</u>), 124.15 (N<u>C</u>), 34.5 (<u>C</u>H_2CH_2<u>C</u>H_2), 30.5 (CH_2<u>C</u>H_2CH_2).

32.4 mg Of the brown powder of **2d** were dissolved in 0.5 mL of $CDCl_3$ containing 6.3 mg of 1,2,4,5-tetrafluorobenzene as internal standard for ^{1}H NMR signals integration. The ratio of the areas of NC<u>H</u> and NCHC<u>H</u> doublets of **1d** and the area of the quintuplet of 1,2,4,5-tetrafluorobenzene revealed that the **1d**/OsO_4 ratio in **2d** is 1:2.

Synthesis and Characterization of 1e·OsO_4 (cocrystal 2e)

The brown powder of co-crystal **2e** was synthetized following the general procedure starting from 0.11 mmol of OsO_4 and 0.10 mmol of 4-methoxypyridine 1-oxide hydrated (**1e·$(H_2O)_n$**, Sigma Aldrich). FTIR (solid, cm^{-1}) 1630, 1494, 1198, 906, 754, 557. ^{1}H NMR (400.13 MHz, $CDCl_3$) δ 8.06 (*d*, J = 8.0 Hz, 2H), 6.78 (*d*, J = 7.2 Hz, 2H), 3.82 (*s*, 3H). ^{13}C NMR (100.61 MHz, $CDCl_3$) δ 159.3 (NCHCH<u>C</u>), 140.7 (NCH<u>C</u>H), 111.7 (N<u>C</u>H), 56.2 (<u>C</u>H_3).
Crystallization of commercially available **1e·$(H_2O)_n$** (Sigma Aldrich) from non-anhydrous CH_2Cl_2 afforded **1e·H_2O** wherein water was hydrogen bonded to *N*-oxide oxygen (Tables S19-24, Figure S19). When **1e·H_2O** and OsO_4 were crystallized following the general procedure, **2e** was isolated in nearly quantitative yields.
26.2 mg Of the brown powder of **2e** were dissolved in 0.5 mL of $CDCl_3$ containing 6.3 mg of 1,2,4,5-tetrafluorobenzene as internal standard for ^{1}H NMR signals integration. The ratio of the areas of NC<u>H</u> and NCHC<u>H</u> doublets of **1e** and the area of the quintuplet of 1,2,4,5-tetrafluorobenzene revealed that the **1e**/OsO_4 ratio in **2e** is 1:1.

Synthesis and Characterization of 1f·OsO_4 (cocrystal 2f)

The brown powder of co-crystal **2f** was synthetized following the general procedure starting from 0.108 mmol of OsO_4 and 0.100 mmol of isoquinoline 1-oxide (**1f**). FTIR (solid, cm^{-1}) 1613, 1428, 1207, 1022, 900, 820, 750, 539. ^{1}H NMR (400.13 MHz, $CDCl_3$) δ 8.70 (*s*, 1H), 8.07 (*dd*, J = 7.2, 1.6 Hz, 1H), 7.71 (*dd*, J = 7.6, 1.52, Hz, 2H), 7.60 (*d*, J = 6.8 Hz, 1H), 7.55 (*m*, J = 7.2 Hz, 1H). ^{13}C NMR (100.61 MHz, $CDCl_3$) δ 136.9 (N<u>C</u>H), 136.3 (N<u>C</u>H), 129.5 (NCH<u>C</u>), 129.1 (NCH<u>C</u>), 126.7 (NCHC<u>C</u>H), 125.0 (NCHC<u>C</u>H), 124.2 (NCHCCH<u>C</u>H).
Crystallization of commercially available **1f** (Sigma Aldrich) from non-anhydrous CH_2Cl_2 afforded hydrated **1f** (Figure S3: IR spectrum). When **1f·$(H_2O)_n$** and OsO_4 were crystallized following the general procedure, **2f** was isolated in nearly quantitative yields.
24.9 mg Of the brown powder of **2f** were dissolved in 0.5 mL of $CDCl_3$ containing 6.3 mg of 1,2,4,5-tetrafluorobenzene as internal standard for ^{1}H NMR signals integration. The ratio of the areas of signals of **1f** and the area of the quintuplet of 1,2,4,5-tetrafluorobenzene revealed that the **1f**/OsO_4 ratio in **2f** is 1:1.

^{1}H and ^{13}C NMR spectra of pure **1a**-**f** are very similar to those reported above for corresponding adducts for **2a**-**f** (differences are at the second decimal for ^{1}H NMR spectra and at the first decimal for ^{13}C NMR spectra).

S2.2 Infrared Spectra

Images of selected solid and solution IR spectra of starting materials **1** and respective osme and hydrogen bonded adducts are reported in Figures S1-S5.

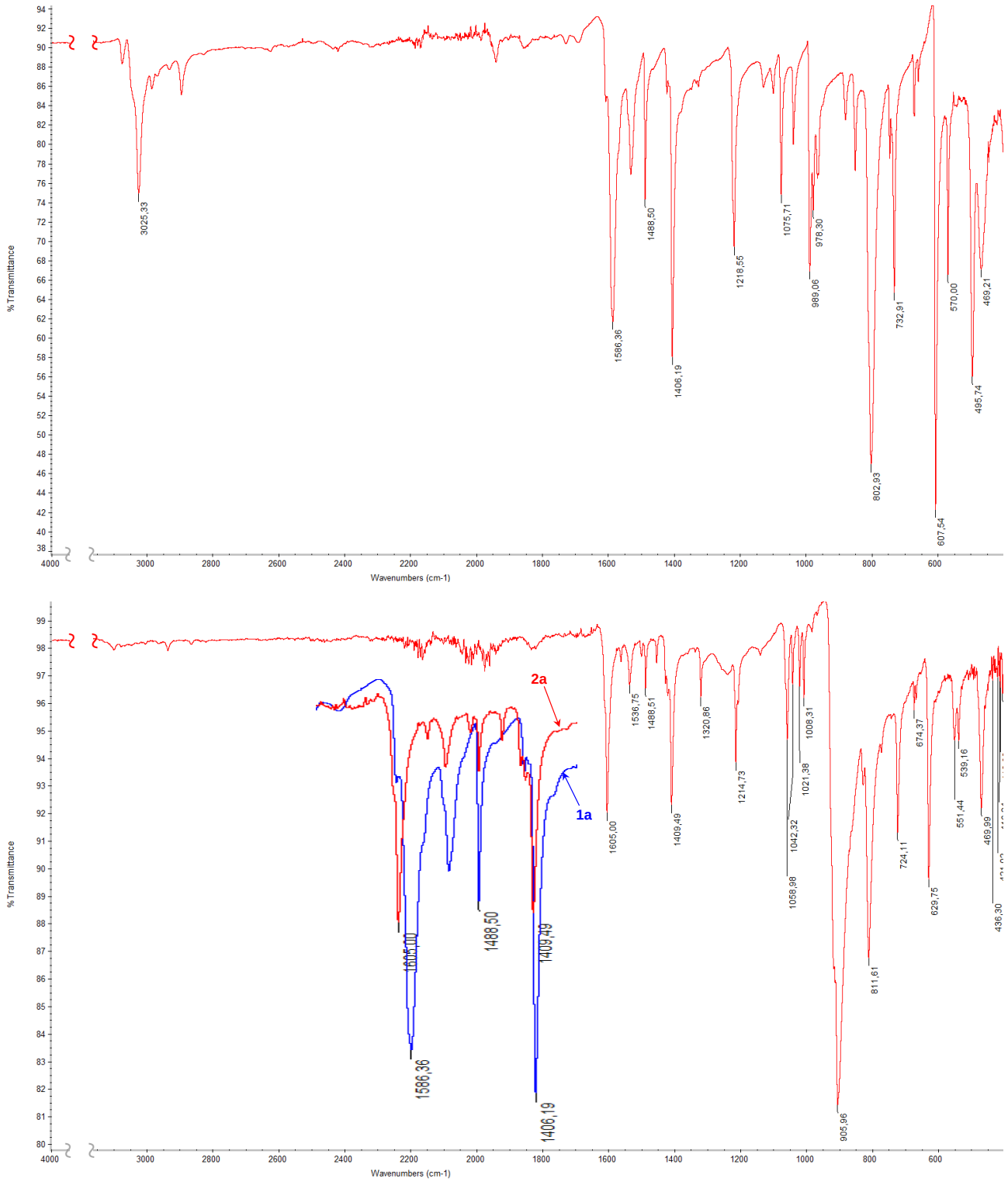

Figure S1. IR spectra (solid) of pure 4,4'-bipyridine (**1a**) (top) and of corresponding cocrystal **1a·(OsO$_4$)$_2$** (**2a**) (bottom). The insert in the bottom spectrum is zooming on overlapped spectra in the region of breathing vibrations.

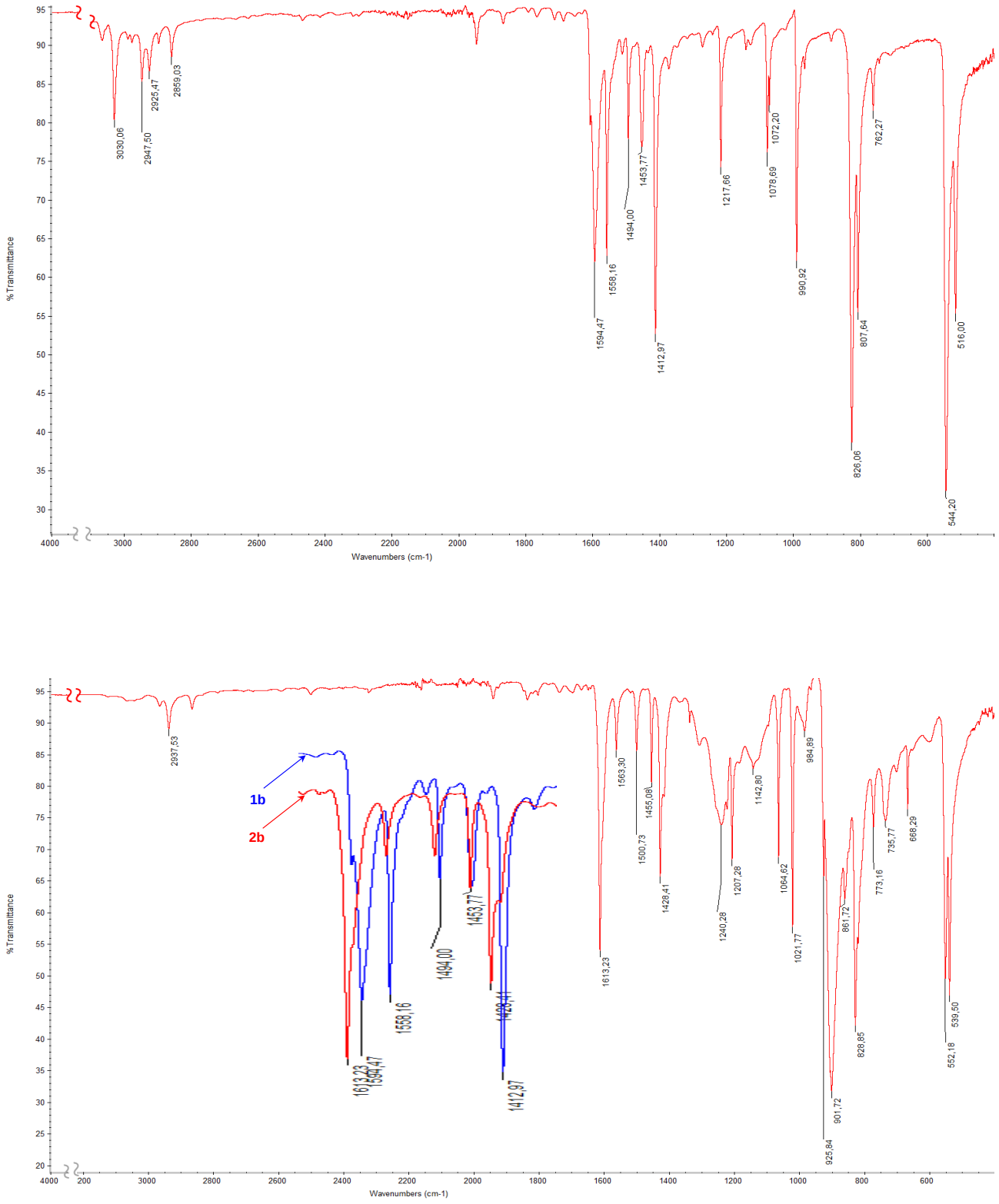

Figure S2. IR spectra (solid) of pure 1,2-di(pyridin-4-yl)ethane (**1b**) (top) and of corresponding cocrystal **1b·(OsO$_4$)$_2$** (**2b**) (bottom). The insert in the bottom spectrum is zooming on overlapped spectra in the region of breathing vibrations.

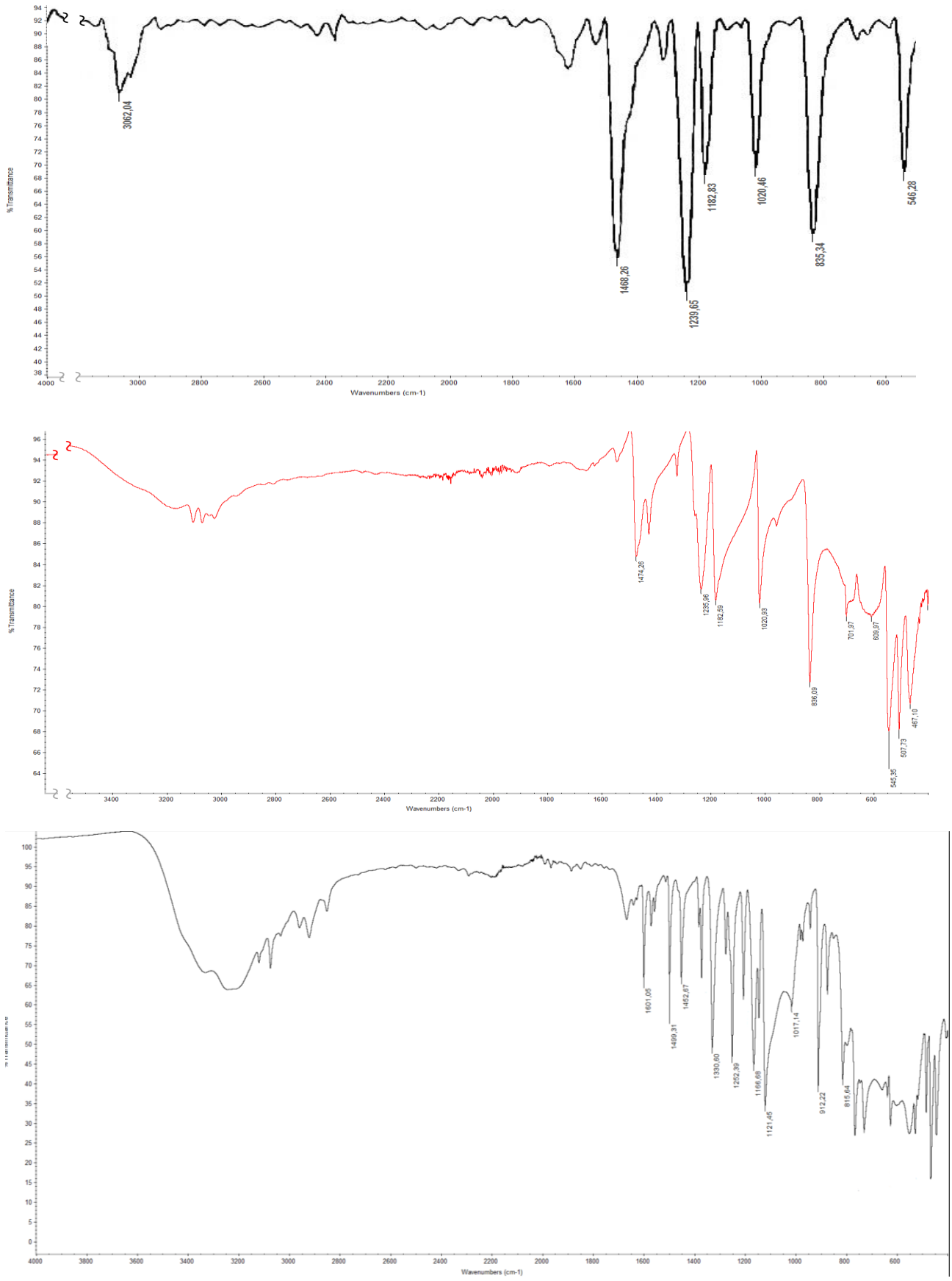

Figure S3. IR spectra (solid) of [4,4'-bipyridine] 1,1'-dioxide (**1c**) (top), [4,4'-bipyridine] 1,1'-dioxide polyhydrate (**1c·(H$_2$O)$_n$**) (mid), isoquinoline 2-oxide hydrated (**1f·(H$_2$O)$_n$**) (bottom).

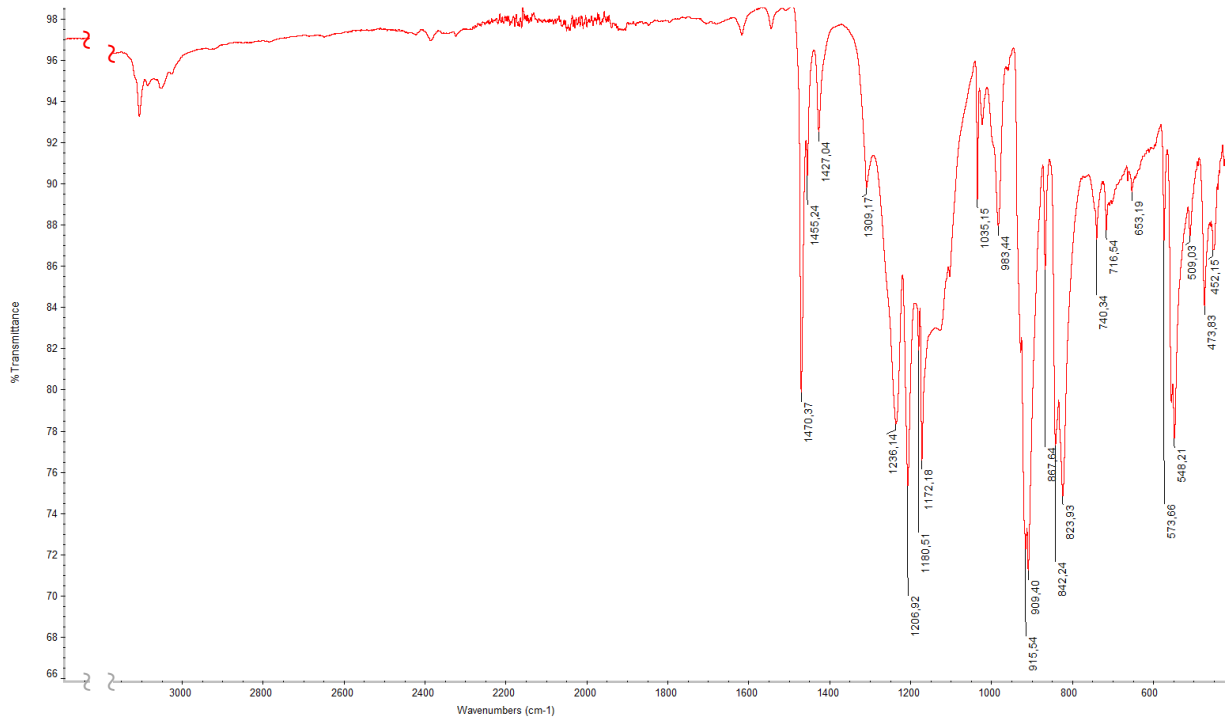

Figure S4. IR spectrum (solid) of the cocrystal **1c·(OsO$_4$)$_2$** (**2c**).

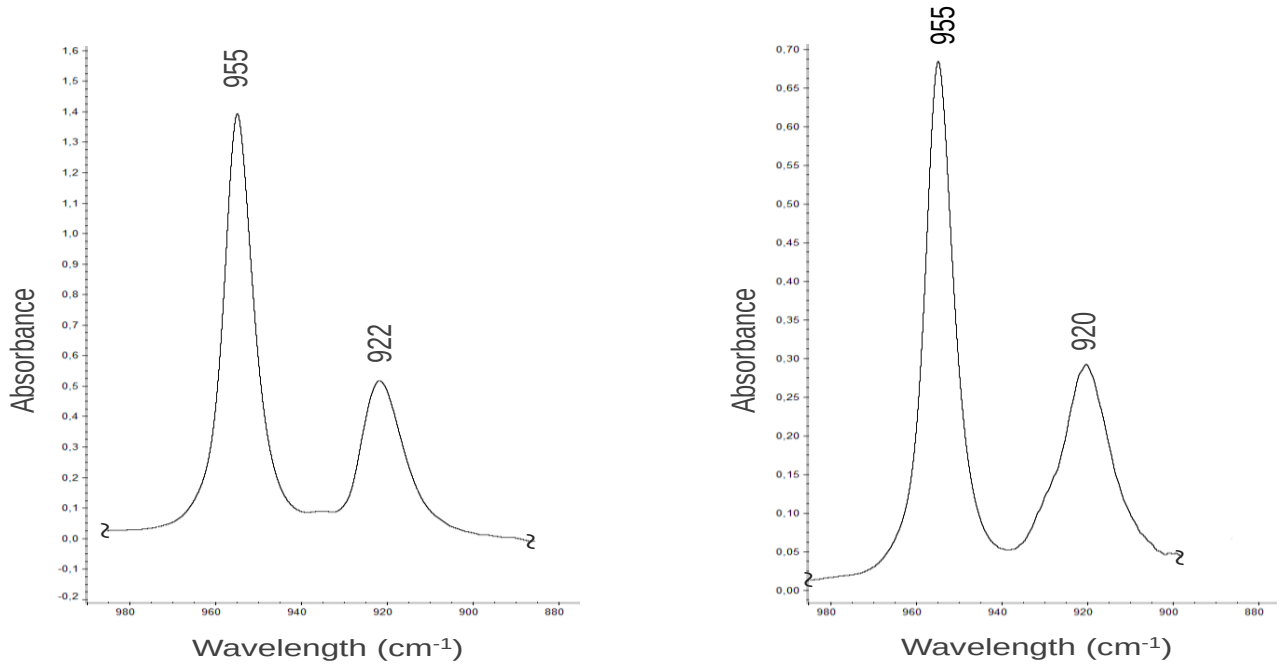

Figure S5. IR spectra ($CHCl_3$ solution) of cocrystals **2a** (left) and **2b** (right) in the region of $\nu 3$ band of OsO_4.

S2.3 NMR Spectra

Images of selected ^{13}C and ^{15}N SSNMR spectra of starting materials **1** and respective osme, hydrogen, halogen, and pnictogen bonded adducts are reported in Figures S6-S15.

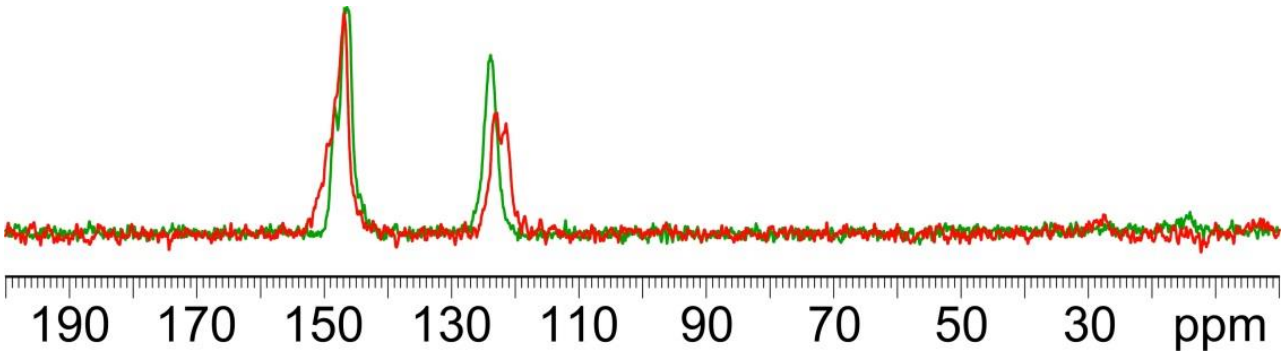

Figure S6. ^{13}C SSNMR spectra of: pure **1a**, red line (121.4 and 122.9, NCHCH; 146.9, NCH and NCHCHC); cocrystal **1a·OsO$_4$·(2a)**, green line (123.8, NCHCH; 146.4, NCH; 148.3, NCHCHC).

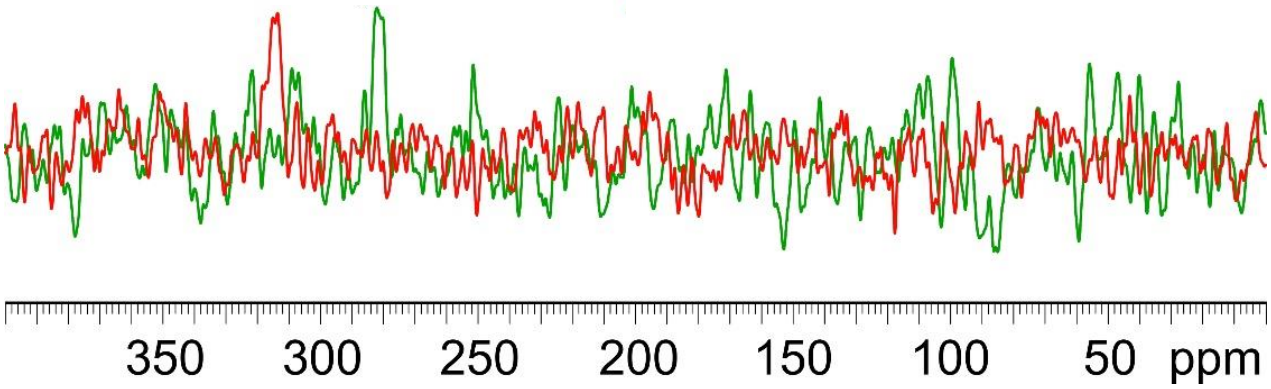

Figure S7. ^{15}N SSNMR spectra of: pure **1a**, red line (313.7); cocrystal **1a·OsO$_4$·(2a)**, green line (282.0).

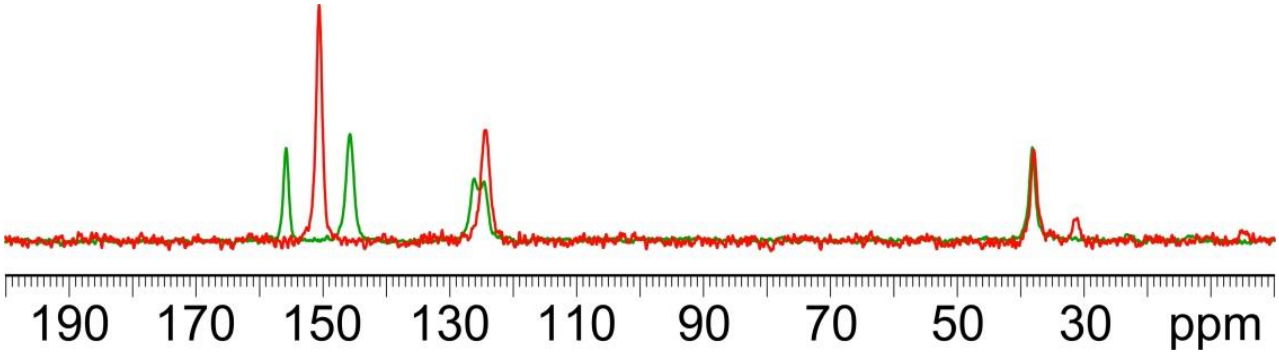

Figure S8. ^{13}C SSNMR spectra of: pure **1b**, red line (38.0, CH_2; 124.6 and 126.2, NCHCH; 150.6, NCH and NCHCHC); cocrystal **1b·OsO$_4$·(2b)**, green line (38.2, CH_2; 123.8, NCHCH; 145.6, NCH; 155.8, NCHCHC).

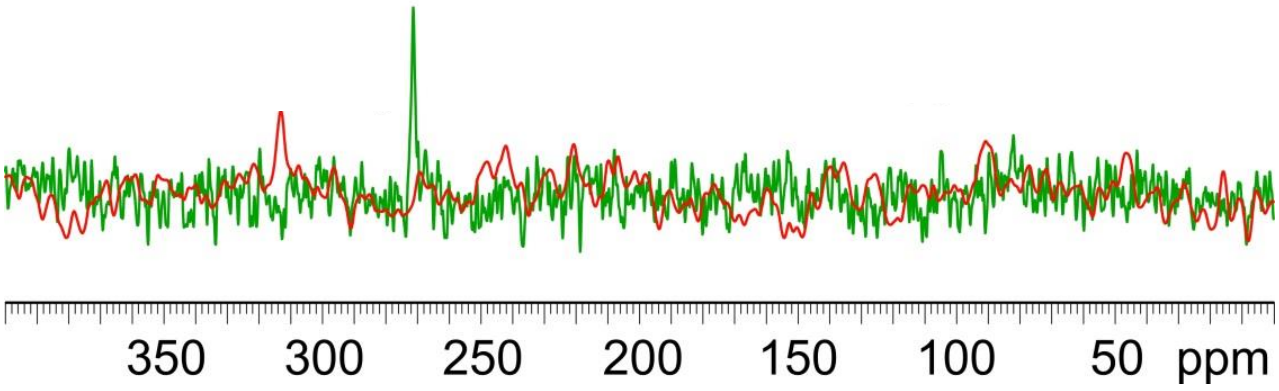

Figure S9. ^{15}N SSNMR spectra of: pure **1b**, red line (313.0); cocrystal **1b·OsO$_4$·(2b)**, green line (271.3).

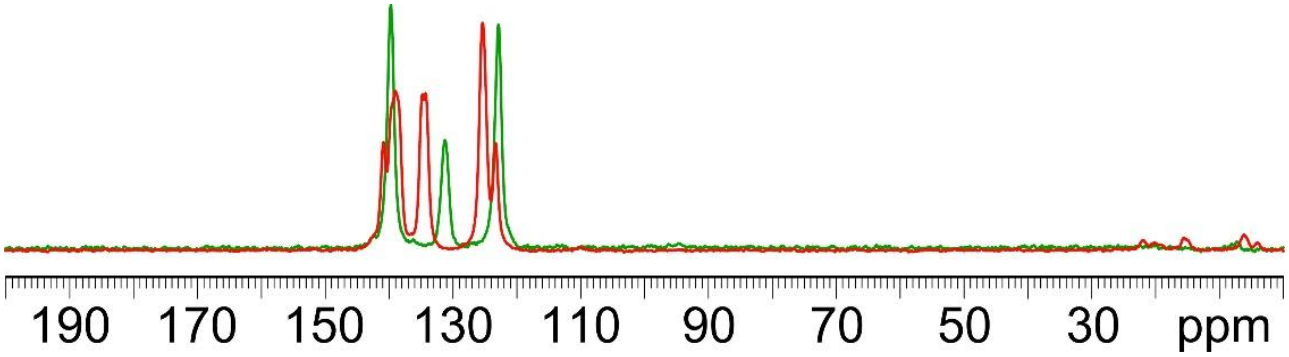

Figure S10. ^{13}C SSNMR spectra of: **1c·(H$_2$O)$_2$**, red line (123.5 and 125.5, NCHCH; 134.5 and 134.9, NCHCHC; 139.2, 139.9 and 141.1, NCH); **1c·OsO$_4$·(2c)**, green line (122.9, NCHCH; 131.3, NCHCHC; 139.7, NCH).

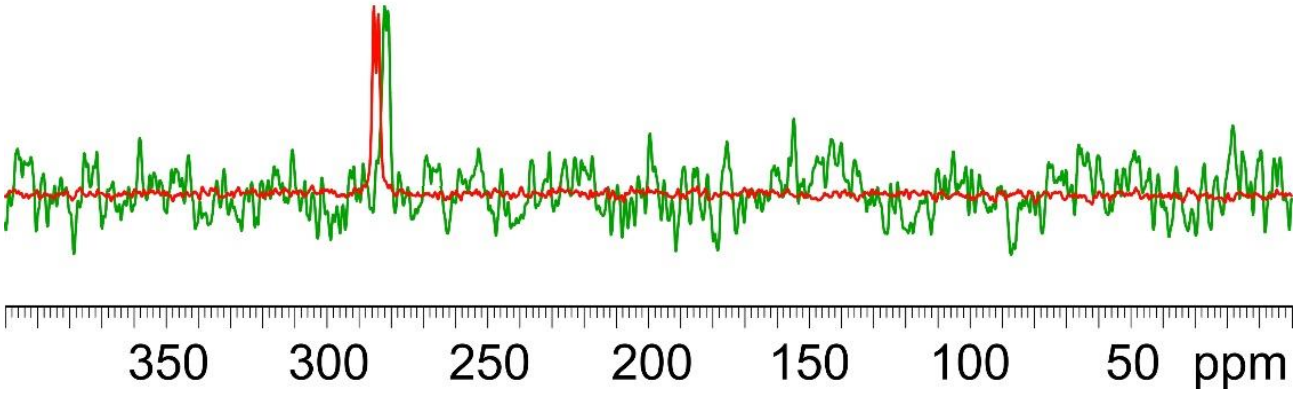

Figure S11. ^{15}N SSNMR spectra of: **1c·(H$_2$O)$_2$**, red line (283.8 and 285.3); **1c·OsO$_4$·(2c)**, green line (280.9 and 282.0).

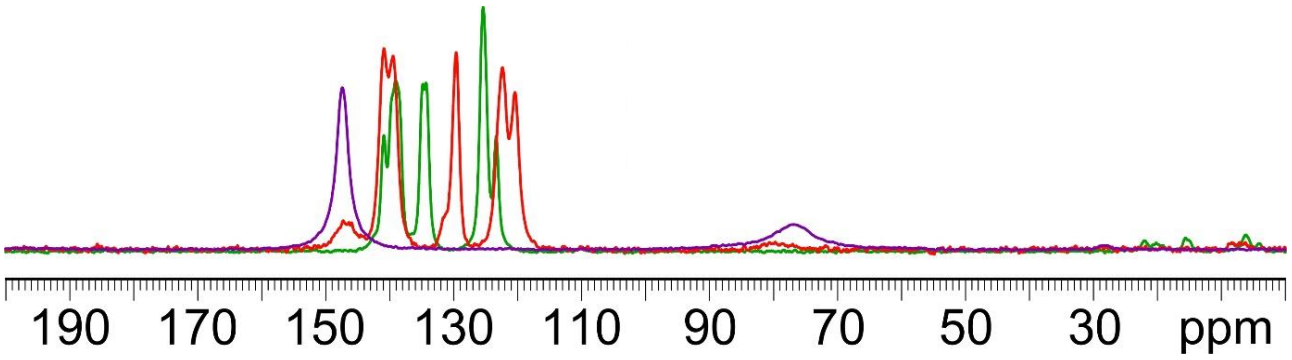

Figure S12. ^{13}C SSNMR spectra of: **1c·(H$_2$O)$_2$**, green line (141.1, 139.9 and 139.2, NCH; 134.9 and 134.5, NCHCHC; 125.5 and 123.5, NCHCH); **1,4-I$_2$-C$_6$F$_4$**, violet line (147.4, CF; 76.8, CI); **1c·1,4-I$_2$-C$_6$F$_4$**, red line (~147, CF; 141.1 and 139.9, NCH; 129.7 NCHCHC; 122.3 and 120.4, NCHCH; ~80, CI).

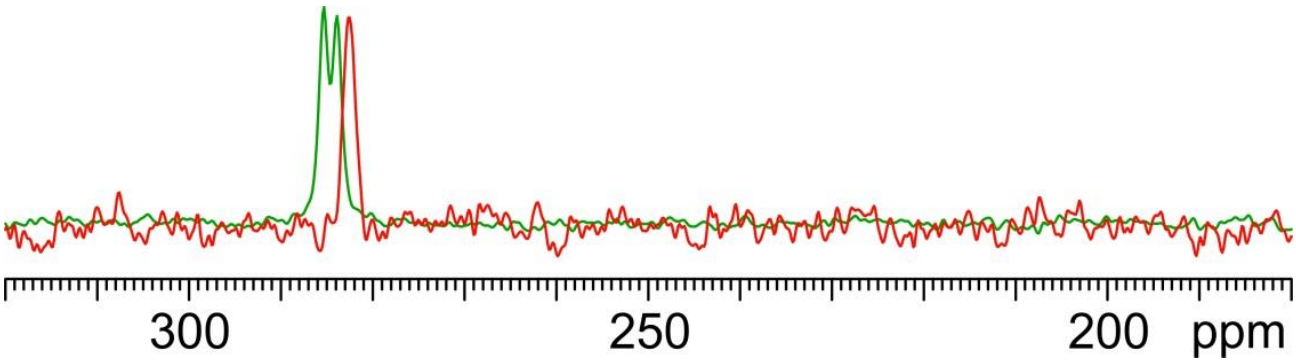

Figure S13. ^{15}N SSNMR spectra of: **1c·(H$_2$O)$_2$**, green line (285.3 and 283.8); **1c·1,4-I$_2$-C$_6$F$_4$**, red line (282.5).

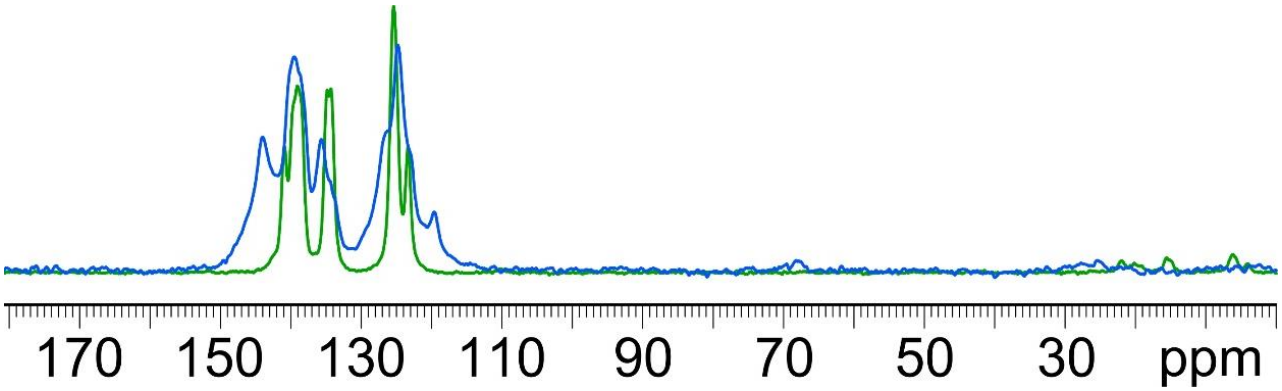

Figure S14. ^{13}C SSNMR spectra of: **1c·(H$_2$O)$_2$**, green line (123.5 and 125.5, NCH<u>C</u>H; 134.5 and 134.9, NCHCH<u>C</u>; 139.2, 139.9 and 141.1, N<u>C</u>H); **1c·SbF$_3$**, blue line (traces of starting **1c·(H$_2$O)$_2$** are present in the sample) (126.7, 124.7 and 119.7, NCH<u>C</u>H; 135.6, NCHCH<u>C</u>; 143.9 and 139.7, N<u>C</u>H).

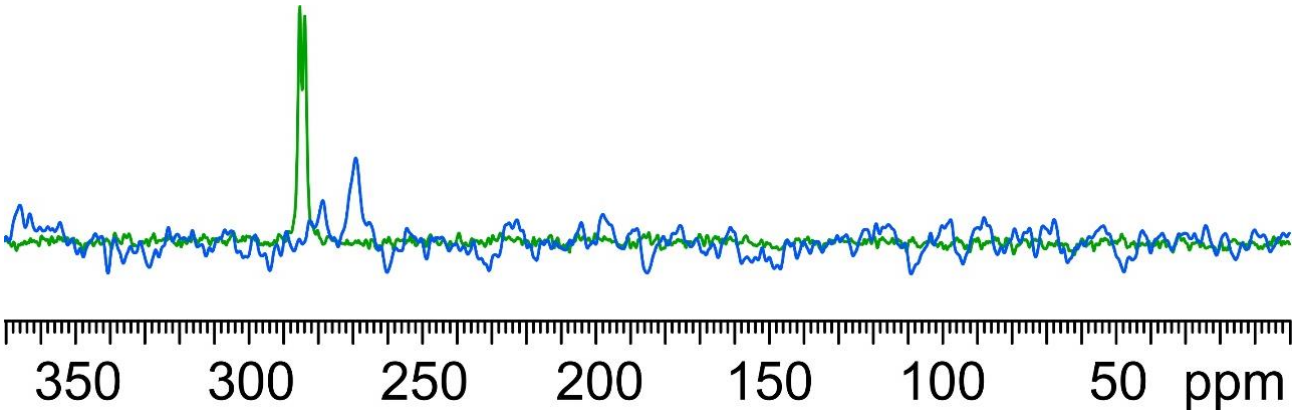

Figure S15. ^{15}N SSNMR spectra of: **1c·(H$_2$O)$_2$**, green line (285.3 and 283.8); **1c·SbF$_3$**, blue line (269.1).

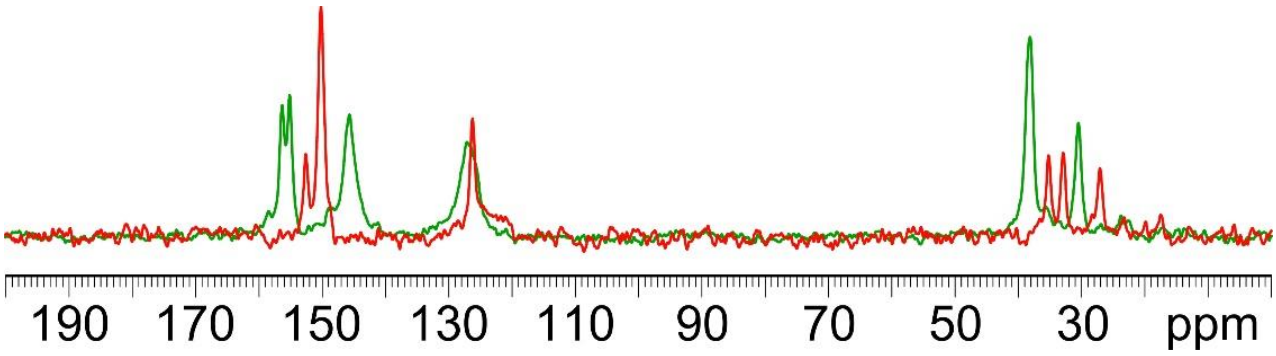

Figure S16. ^{13}C SSNMR spectra of: pure **1d**, red line (27.1.0, $NC_5H_4CH_2\underline{C}H_2$; 32.8 and 35.2, $NC_5H_4\underline{C}H_2$; 126.2, NCH<u>C</u>H; 150.1, N<u>C</u>H; 152.6, NCHCH<u>C</u>); cocrystal **1d·OsO_4·(2d)**, green line (30.5, $NC_5H_4CH_2\underline{C}H_2$; 38.1, $NC_5H_4\underline{C}H_2$; 127.0, NCH<u>C</u>H; 145.6, N<u>C</u>H; 155.1 and 156.3, NCHCH<u>C</u>).

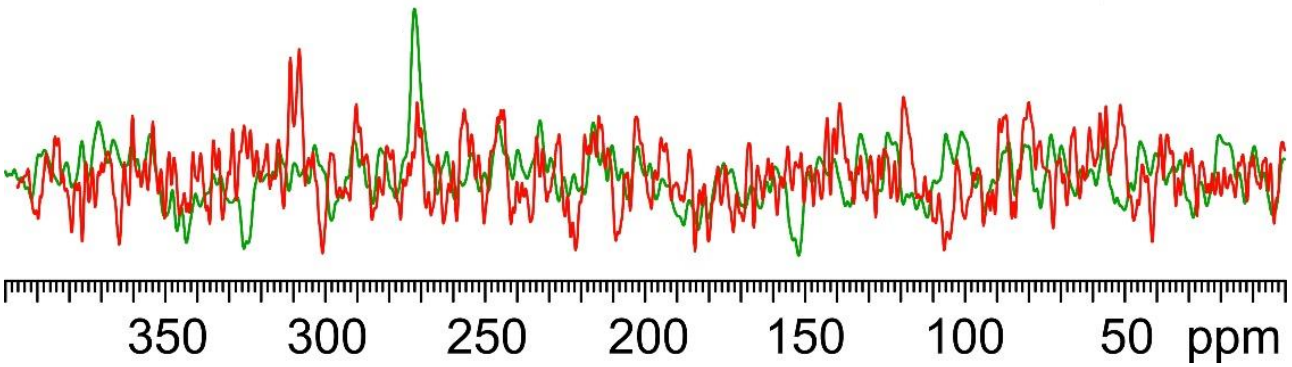

Figure S17. ^{15}N SSNMR spectra of: pure **1d**, red line (310.9 and 308.2); cocrystal **1d·OsO_4·(2d)**, green line (272.1).

S3. Crystallographic data.

S3.1 van der Waals radii and their reliability

Traditional Bondi's values were used for the van der Waals radii of N and O (155 and 152 pm, respectively)[6] and the conservative Batsanov's value is employed for Os (200 pm).[7] It is commonly assumed that Nc values smaller than 1 indicate an interaction between the involved atoms. There are limitations to the validity of this assumption. For instance, atoms in molecules are not spherical, radii along the extension of covalent bonds are usually less than perpendicular to the bonds.[8-14] Uncertainty in van der Waals radii of metals is particularly high (e.g., values as high as 235 pm were proposed for Os)[15] and the size of any element depends on its oxidation state. The analysis based on van der Waals radii is nevertheless adopted here as it is the universally employed approach to identify the hallmarks of the landscape of intermolecular interactions present in a crystal packing.

Table S1. Crystal data and structure refinement for **2a**.

Identification code	**2a**
Empirical formula	$C_{20}H_{16}N_4O_{16}Os_4$
Formula weight	1329.17
Temperature/K	100(2)
Crystal system	tetragonal
Space group	$P4_2/mbc$
a/Å	14.4805(13)
b/Å	14.4805(13)
c/Å	6.4815(6)
α/°	90
β/°	90
γ/°	90
Volume/Å^3	1359.1(3)
Z	2
ρ_{calc}g/cm^3	3.248
μ/mm^{-1}	18.724
F(000)	1192.0
Crystal size/mm^3	0.08 × 0.02 × 0.02
Radiation	MoKα (λ = 0.71073)
2Θ range for data collection/°	6.292 to 54.576
Index ranges	-18 ≤ h ≤ 18, -18 ≤ k ≤ 18, -8 ≤ l ≤ 8
Reflections collected	22626
Independent reflections	828 [R_{int} = 0.1065, R_{sigma} = 0.0255]
Data/restraints/parameters	828/0/64
Goodness-of-fit on F^2	0.817
Final R indexes [I>=2σ (I)]	R_1 = 0.0196, wR_2 = 0.0560
Final R indexes [all data]	R_1 = 0.0283, wR_2 = 0.0603
Largest diff. peak/hole / e Å^{-3}	1.06/-1.29
CCDC num.	2089899

Table S2. Fractional Atomic Coordinates ($\times 10^4$) and Equivalent Isotropic Displacement Parameters ($Å^2 \times 10^3$) for **2a**. U_{eq} is defined as 1/3 of of the trace of the orthogonalised U_{IJ} tensor.

Atom	*x*	*y*	*z*	U(eq)
Os1	6137.9(2)	3624.9(2)	0	18.65(13)
N1	7686(4)	4206(3)	0	12.7(11)
C3	8393(4)	3602(4)	0	11.6(12)
C2	9311(4)	3907(4)	0	14.3(14)
C1	9512(4)	4836(4)	0	11.5(12)
O2	5958(3)	4792(3)	0	25.5(12)
O1	6576(2)	3144(3)	2229(6)	32.2(9)
C4	8765(4)	5452(5)	0	13.7(13)
C5	7873(5)	5108(4)	0	16.4(14)
O3	5032(3)	3203(3)	0	34.6(14)

Table S3. Anisotropic Displacement Parameters ($Å^2 \times 10^3$) for **2a**. The Anisotropic displacement factor exponent takes the form: $-2\pi^2[h^2a^{*2}U_{11}+2hka^*b^*U_{12}+\ldots]$.

Atom	U_{11}	U_{22}	U_{33}	U_{23}	U_{13}	U_{12}
Os1	11.01(17)	12.24(18)	32.7(2)	0	0	-1.41(9)
N1	14(3)	14(3)	10(3)	0	0	-3(2)
C3	15(3)	8(3)	12(3)	0	0	-1(2)
C2	17(3)	10(3)	16(3)	0	0	2(2)
C1	13(3)	15(3)	6(3)	0	0	2(2)
O2	13(2)	13(2)	50(3)	0	0	0.2(19)
O1	22.3(18)	35(2)	39(3)	16.6(17)	3.2(16)	-3.1(16)
C4	13(3)	11(3)	17(3)	0	0	-1(2)
C5	18(4)	9(3)	22(4)	0	0	2(2)
O3	18(3)	20(3)	66(4)	0	0	-6(2)

Table S4. Bond Lengths for **2a**.

Atom	Atom	Length/Å	Atom	Atom	Length/Å
Os1	N1	2.394(5)	N1	C5	1.334(8)
Os1	O2	1.710(5)	C3	C2	1.402(9)
Os1	O1	1.724(4)	C2	C1	1.376(8)
Os1	$O1^1$	1.724(4)	C1	$C1^2$	1.490(12)
Os1	O3	1.714(5)	C1	C4	1.402(8)
N1	C3	1.346(8)	C4	C5	1.385(9)

Table S5. Bond Angles for **2a**.

Atom	Atom	Atom	Angle/˚	Atom	Atom	Atom	Angle/˚
O2	Os1	N1	78.22(19)	C3	N1	Os1	119.0(4)
O2	Os1	$O1^1$	117.06(14)	C3	N1	C5	118.8(6)
O2	Os1	O1	117.06(14)	C5	N1	Os1	122.3(4)
O2	Os1	O3	102.1(2)	N1	C3	C2	121.1(6)
O1	Os1	N1	78.31(12)	C1	C2	C3	120.6(6)
$O1^1$	Os1	N1	78.31(12)	C2	C1	$C1^2$	120.8(7)
$O1^1$	Os1	O1	113.8(3)	C2	C1	C4	117.3(6)
O3	Os1	N1	179.7(2)	C4	C1	$C1^2$	121.9(7)
O3	Os1	$O1^1$	101.54(15)	C5	C4	C1	119.4(6)
O3	Os1	O1	101.54(15)	N1	C5	C4	122.8(6)

Table S6. Hydrogen Atom Coordinates (Å×10^4) and Isotropic Displacement Parameters (Å^2×10^3) for **1**.

Atom	*x*	*y*	*z*	U(eq)
H3	8269.71	2971.87	0	14
H2	9789.27	3478.22	0	17
H4	8868.05	6085.64	0	16
H5	7382.76	5523.05	0	20

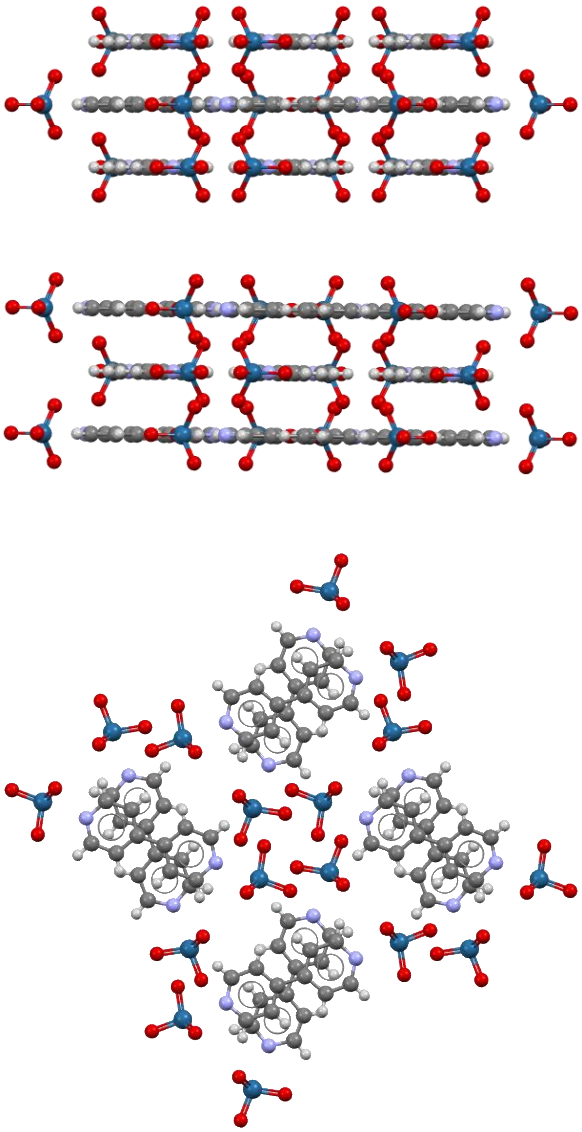

Figure S18. Packing of structure **2a** from *a* axis (top), *b* axis (mid), *c* axis (bottom).

Table S7. Crystal data and structure refinement for **2b**.

Identification code	**2b**
Empirical formula	$C_{12}H_{12}N_2O_8Os_2$
Formula weight	692.64
Temperature/K	100(2)
Crystal system	monoclinic
Space group	$P2_1/c$
a/Å	8.3593(4)
b/Å	12.0646(6)
c/Å	8.8811(4)
α/°	90
β/°	114.514(2)
γ/°	90
Volume/Å^3	814.94(7)
Z	2
ρ_{calc}g/cm^3	2.823
μ/mm^{-1}	15.620
F(000)	628.0
Crystal size/mm^3	0.06 × 0.04 × 0.02
Radiation	MoKα (λ = 0.71073)
2Θ range for data collection/°	6.566 to 55.68
Index ranges	-10 ≤ h ≤ 10, -15 ≤ k ≤ 15, -11 ≤ l ≤ 11
Reflections collected	14445
Independent reflections	1923 [R_{int} = 0.0573, R_{sigma} = 0.0356]
Data/restraints/parameters	1923/0/109
Goodness-of-fit on F^2	1.027
Final R indexes [I>=2σ (I)]	R_1 = 0.0271, wR_2 = 0.0576
Final R indexes [all data]	R_1 = 0.0431, wR_2 = 0.0634
Largest diff. peak/hole / e Å^{-3}	0.96/-0.95
CCDC num.	2089901

Table S8. Fractional Atomic Coordinates (×10^4) and Equivalent Isotropic Displacement Parameters (Å^2×10^3) for **2b**. U_{eq} is defined as 1/3 of of the trace of the orthogonalised U_{IJ} tensor.

Atom	***x***	***y***	***z***	**U(eq)**
Os1	6390.1(3)	1535.5(2)	4620.3(3)	41.82(10)
O1	5770(7)	1047(5)	6099(6)	66.0(14)
O4	8193(6)	728(5)	4963(6)	68.0(15)
O3	7290(6)	2817(4)	4950(8)	80.7(18)
O2	5045(7)	1223(4)	2656(6)	69.1(15)
N1	3892(6)	2656(4)	4179(5)	36.7(11)
C6	-227(7)	4807(5)	4110(7)	43.0(14)
C3	1138(7)	4044(5)	4038(7)	37.3(13)
C1	3835(8)	3730(5)	3754(8)	43.4(14)
C4	1196(8)	2922(6)	4438(8)	49.1(16)
C2	2489(8)	4424(5)	3666(7)	43.0(14)

Atom	*x*	*y*	*z*	U(eq)
C5	2580(8)	2276(5)	4503(8)	45.2(15)

Table S9. Anisotropic Displacement Parameters ($Å^2×10^3$) for **2b**. The Anisotropic displacement factor exponent takes the form: $-2π^2[h^2a^{*2}U_{11}+2hka^*b^*U_{12}+…]$.

Atom	U_{11}	U_{22}	U_{33}	U_{23}	U_{13}	U_{12}
Os1	43.79(15)	43.12(16)	42.40(15)	0.16(12)	21.72(11)	8.19(11)
O1	68(3)	86(4)	54(3)	32(3)	36(2)	31(3)
O4	59(3)	71(4)	72(3)	4(3)	25(3)	28(3)
O3	46(3)	59(3)	150(6)	-16(3)	54(3)	-6(2)
O2	82(4)	72(4)	48(3)	-7(2)	22(3)	29(3)
N1	37(3)	37(3)	39(3)	-4(2)	19(2)	2(2)
C6	31(3)	52(4)	42(3)	-4(3)	11(3)	8(3)
C3	31(3)	42(3)	36(3)	-5(3)	11(2)	5(2)
C1	50(4)	43(4)	49(3)	1(3)	32(3)	4(3)
C4	39(3)	49(4)	66(4)	-5(3)	29(3)	-7(3)
C2	59(4)	36(3)	46(3)	4(3)	34(3)	6(3)
C5	43(3)	34(3)	63(4)	-3(3)	26(3)	-1(3)

Table S10. Bond Lengths for **2b**.

Atom	Atom	Length/Å	Atom	Atom	Length/Å
Os1	O1	1.705(4)	C6	$C6^1$	1.537(11)
Os1	O4	1.713(5)	C6	C3	1.488(8)
Os1	O3	1.691(5)	C3	C4	1.395(9)
Os1	O2	1.680(5)	C3	C2	1.380(8)
Os1	N1	2.380(4)	C1	C2	1.379(8)
N1	C1	1.345(7)	C4	C5	1.376(8)
N1	C5	1.326(7)			

Table S11. Bond Angles for **2b**.

Atom	Atom	Atom	Angle/˚	Atom	Atom	Atom	Angle/˚
O1	Os1	O4	101.1(2)	C5	N1	Os1	121.0(4)
O1	Os1	N1	78.3(2)	C5	N1	C1	117.3(5)
O4	Os1	N1	179.3(2)	C3	C6	$C6^1$	111.4(6)
O3	Os1	O1	116.0(3)	C4	C3	C6	122.4(5)
O3	Os1	O4	101.2(2)	C2	C3	C6	121.5(6)
O3	Os1	N1	78.82(19)	C2	C3	C4	116.0(5)
O2	Os1	O1	115.9(3)	N1	C1	C2	122.2(6)
O2	Os1	O4	102.6(2)	C5	C4	C3	120.0(6)
O2	Os1	O3	116.3(3)	C1	C2	C3	120.9(6)

Atom	Atom	Atom	Angle/˚	Atom	Atom	Atom	Angle/˚
O2	Os1	N1	78.0(2)	N1	C5	C4	123.4(6)
C1	N1	Os1	121.3(4)				

Table S12. Hydrogen Atom Coordinates (Å×10^4) and Isotropic Displacement Parameters (Å^2×10^3) for **2b**.

Atom	*x*	*Y*	*z*	U(eq)
H6A	-1354.63	4431.49	3679.76	52
H6AB	-326.56	5447.46	3416.2	52
H1	4734.61	4013.91	3509.73	52
H4	299.8	2610.3	4661.22	59
H2	2491.75	5159.28	3352.39	52
H5	2596.43	1532.91	4789.54	54

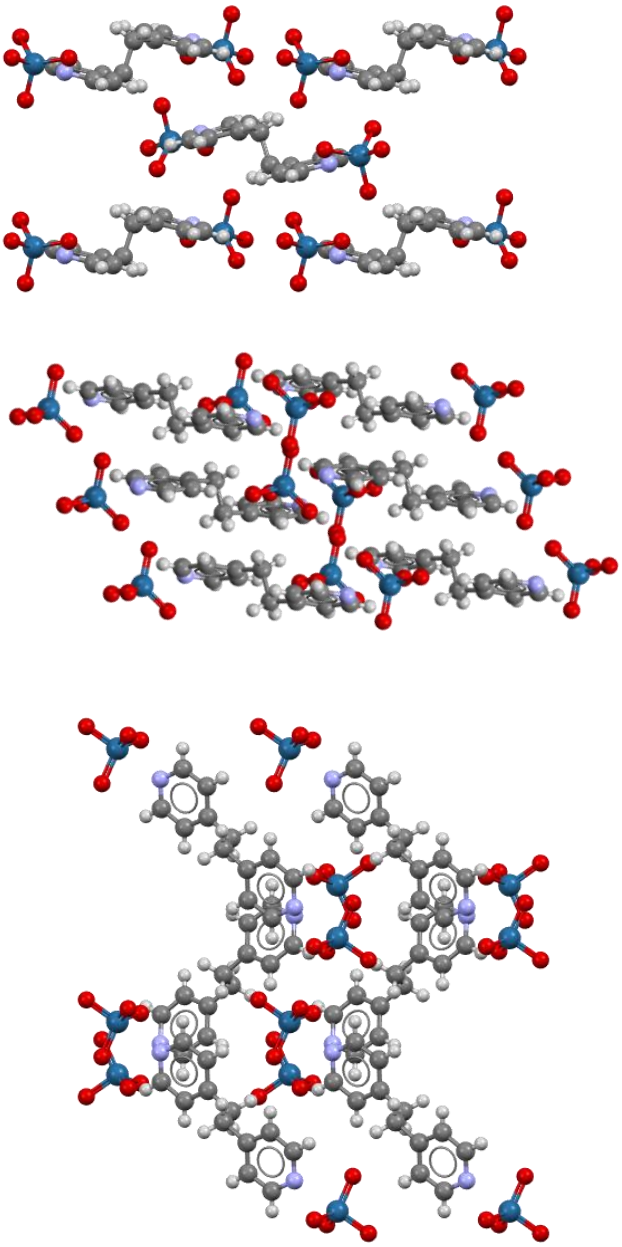

Figure S19. Packing of structure **2b** from *a* axis (top), *b* axis (mid), *c* axis (bottom).

Table S13. Crystal data and structure refinement for **2c**.

Identification code	**2c**
Empirical formula	$C_{10}H_8N_2O_{10}Os_2$
Formula weight	696.58
Temperature/K	100(2)
Crystal system	monoclinic
Space group	$P2_1/n$
a/Å	13.2536(16)
b/Å	7.5785(9)
c/Å	15.7024(19)
α/°	90
β/°	112.724(7)
γ/°	90
Volume/Å^3	1454.8(3)
Z	4
ρ_{calc}g/cm^3	3.180
μ/mm^{-1}	17.511
F(000)	1256.0
Crystal size/mm^3	0.1 × 0.04 × 0.02
Radiation	MoKα (λ = 0.71073)
2Θ range for data collection/°	6.326 to 56.332
Index ranges	-17 ≤ h ≤ 17, -10 ≤ k ≤ 9, -20 ≤ l ≤ 17
Reflections collected	13650
Independent reflections	3546 [R_{int} = 0.0552, R_{sigma} = 0.0554]
Data/restraints/parameters	3546/0/217
Goodness-of-fit on F^2	1.013
Final R indexes [I>=2σ (I)]	R_1 = 0.0316, Wr_2 = 0.0497
Final R indexes [all data]	R_1 = 0.0523, Wr_2 = 0.0542
Largest diff. Peak/hole / e Å^{-3}	3.12/-2.09
CCDC num	2089902

Table S14. Fractional Atomic Coordinates (×10^4) and Equivalent Isotropic Displacement Parameters (Å^2×10^3) for **2c**. U_{eq} is defined as 1/3 of of the trace of the orthogonalised U_{IJ} tensor.

Atom	***x***	***y***	***z***	**U(eq)**
Os1	9019.3(2)	10214.5(3)	-2227.9(2)	12.91(7)
Os2	4907.1(2)	-522.7(4)	1450.1(2)	18.74(8)
C5	5995(6)	4175(8)	1250(5)	17.4(15)
C2	7874(5)	3005(9)	1123(4)	15.0(15)
C1	7420(5)	4586(8)	706(4)	13.3(13)
N3	6465(4)	2683(7)	1683(4)	11.4(12)
C3	7384(5)	2072(9)	1615(5)	19.0(16)
C6	6469(5)	5169(9)	782(5)	15.9(14)
O1	4409(4)	1073(7)	629(3)	22.4(11)
O2	4072(5)	-2278(7)	958(4)	39.4(16)
O3	4718(4)	-229(6)	2460(3)	24.0(12)
O4	6168(4)	-1333(7)	1570(3)	27.6(13)

Atom	*x*	*y*	*z*	U(eq)
O6	8555(4)	11545(6)	-3187(3)	20.7(11)
O5	8083(4)	8540(7)	-2536(3)	22.9(12)
O7	8963(4)	11528(6)	-1365(3)	26.2(12)
O8	6028(4)	1793(6)	2195(3)	17.9(10)
O9	10306(3)	9693(6)	-2153(3)	18.9(11)
O10	9787(3)	8318(6)	-944(3)	14.6(10)
N2	9133(4)	7480(7)	-616(4)	12.1(12)
C7	7973(5)	5622(9)	212(4)	11.2(13)
C9	8149(5)	7431(9)	354(4)	13.3(14)
C10	8374(5)	4801(9)	-383(4)	13.2(13)
C8	8725(5)	8339(9)	-56(4)	13.2(14)
C11	8925(5)	5749(8)	-813(4)	14.8(15)

Table S15. Anisotropic Displacement Parameters ($Å^2 \times 10^3$) for **2c**. The Anisotropic displacement factor exponent takes the form: $-2\pi^2[h^2a^{*2}U_{11}+2hka^*b^*U_{12}+\ldots]$.

Atom	U_{11}	U_{22}	U_{33}	U_{23}	U_{13}	U_{12}
Os1	12.31(12)	12.63(14)	11.75(13)	0.64(11)	2.40(9)	-0.62(10)
Os2	27.12(16)	13.92(15)	14.34(15)	1.48(12)	7.09(12)	-2.84(12)
C5	21(4)	9(3)	25(4)	-6(3)	12(3)	3(3)
C2	12(3)	20(4)	9(3)	3(3)	-1(3)	-2(3)
C1	18(3)	9(3)	12(3)	1(3)	4(3)	-3(3)
N3	17(3)	8(3)	9(3)	-1(2)	6(2)	-3(2)
C3	16(4)	18(4)	23(4)	5(3)	8(3)	4(3)
C6	22(3)	8(3)	18(4)	-3(3)	9(3)	-1(3)
O1	25(3)	25(3)	15(3)	0(2)	6(2)	0(2)
O2	57(4)	31(3)	26(3)	-5(3)	12(3)	-26(3)
O3	30(3)	24(3)	22(3)	3(2)	14(2)	-9(2)
O4	40(3)	19(3)	24(3)	2(2)	11(3)	9(2)
O6	19(3)	17(3)	20(3)	4(2)	1(2)	-3(2)
O5	20(3)	27(3)	17(3)	7(2)	2(2)	-8(2)
O7	34(3)	21(3)	19(3)	0(2)	5(2)	14(2)
O8	26(3)	19(3)	13(3)	2(2)	12(2)	-3(2)
O9	14(2)	19(3)	24(3)	7(2)	9(2)	1(2)
O10	12(2)	17(3)	14(3)	8(2)	4.2(19)	0.9(19)
N2	10(3)	13(3)	8(3)	3(2)	-2(2)	-3(2)
C7	9(3)	15(4)	8(3)	2(3)	2(2)	0(2)
C9	17(3)	11(4)	11(3)	-4(3)	4(3)	0(3)
C10	17(3)	11(3)	10(3)	2(3)	3(3)	2(3)
C8	12(3)	15(4)	10(3)	-8(3)	2(3)	-2(3)
C11	16(3)	13(4)	9(3)	-2(3)	-2(3)	8(3)

Table S16. Bond Lengths for **2c**.

Atom	Atom	Length/Å	Atom	Atom	Length/Å
Os1	O6	1.717(5)	C2	C3	1.381(9)
Os1	O5	1.709(5)	C1	C6	1.383(9)
Os1	O7	1.706(5)	C1	C7	1.482(9)
Os1	O9	1.709(4)	N3	C3	1.345(8)
Os1	O10	2.362(4)	N3	O8	1.341(6)
Os2	O1	1.703(5)	O10	N2	1.329(6)
Os2	O2	1.712(5)	N2	C8	1.362(8)
Os2	O3	1.712(5)	N2	C11	1.351(8)
Os2	O4	1.721(5)	C7	C9	1.394(9)
Os2	O8	2.305(5)	C7	C10	1.388(9)
C5	N3	1.343(8)	C9	C8	1.360(9)
C5	C6	1.363(9)	C10	C11	1.374(9)
C2	C1	1.386(9)			

Table S17. Bond Angles for **2c**.

Atom	Atom	Atom	Angle/˚	Atom	Atom	Atom	Angle/˚
O6	Os1	O10	174.99(19)	C3	C2	C1	119.6(6)
O5	Os1	O6	102.3(2)	C2	C1	C7	119.5(6)
O5	Os1	O9	116.3(2)	C6	C1	C2	118.7(6)
O5	Os1	O10	79.41(19)	C6	C1	C7	121.8(6)
O7	Os1	O6	104.1(2)	C5	N3	C3	120.5(6)
O7	Os1	O5	114.1(2)	O8	N3	C5	120.2(5)
O7	Os1	O9	115.4(2)	O8	N3	C3	119.3(5)
O7	Os1	O10	79.3(2)	N3	C3	C2	120.2(6)
O9	Os1	O6	101.9(2)	C5	C6	C1	119.7(6)
O9	Os1	O10	73.19(18)	N3	O8	Os2	114.9(3)
O1	Os2	O2	102.5(2)	N2	O10	Os1	119.4(3)
O1	Os2	O3	117.1(2)	O10	N2	C8	120.2(5)
O1	Os2	O4	114.4(2)	O10	N2	C11	118.7(5)
O1	Os2	O8	80.2(2)	C11	N2	C8	121.0(6)
O2	Os2	O3	102.7(2)	C9	C7	C1	121.5(6)
O2	Os2	O4	101.7(3)	C10	C7	C1	120.7(6)
O2	Os2	O8	176.6(2)	C10	C7	C9	117.7(6)
O3	Os2	O4	115.3(2)	C8	C9	C7	120.8(6)
O3	Os2	O8	74.15(19)	C11	C10	C7	120.8(6)
O4	Os2	O8	78.9(2)	C9	C8	N2	120.0(6)
N3	C5	C6	121.2(6)	N2	C11	C10	119.7(6)

Table S18. Hydrogen Atom Coordinates (Å×10^4) and Isotropic Displacement Parameters (Å^2×10^3) for **2c**.

Atom	*x*	*y*	*z*	U(eq)
H5	5333.64	4537.65	1269.46	21
H2	8505.38	2576.03	1070.96	18
H3	7690.58	1016.48	1900.71	23
H6	6155.08	6233.56	515.55	19
H9	7869.01	8024.62	732.85	16
H10	8267.65	3595.99	-492.51	16
H8	8840.57	9544.12	45.58	16
H11	9155.03	5202.66	-1237.7	18

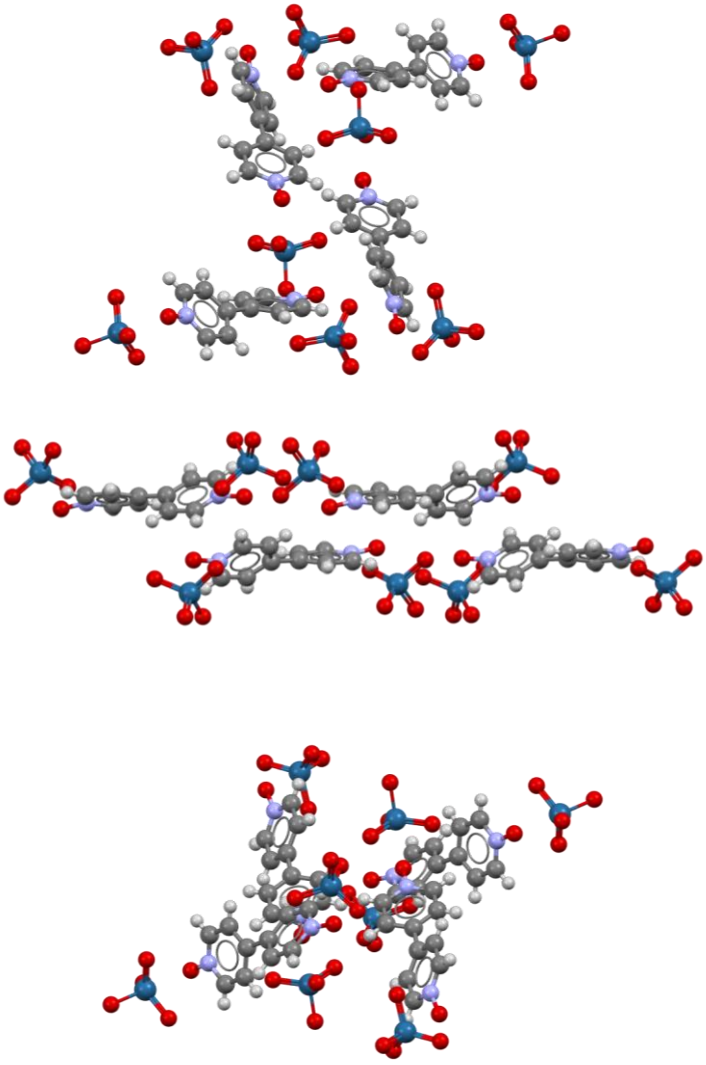

Figure S20. Packing of structure **2c** from *a* axis (top), *b* axis (mid), *c* axis (bottom).

Table S19. Crystal data and structure refinement for **1e·H_2O**.

Identification code	**1e·H_2O**
Empirical formula	$C_6H_8NO_{2.5}$
Formula weight	134.13
Temperature/K	296(2)
Crystal system	monoclinic
Space group	C2/c
a/Å	13.50(7)
b/Å	6.46(3)
c/Å	14.79(5)
α/°	90
β/°	100.11(18)
γ/°	90
Volume/Å^3	1270(10)
Z	8
ρ_{calc}g/cm^3	1.404
μ/mm^{-1}	0.110
F(000)	568.0
Crystal size/mm^3	0.8 × 0.4 × 0.2
Radiation	MoKα (λ = 0.71073)
2Θ range for data collection/°	6.132 to 40.618
Reflections collected	568
Independent reflections	568 [R_{int} = 0.068, R_{sigma} = 0.0271]
Data/restraints/parameters	568/0/92
Goodness-of-fit on F^2	1.199
Final R indexes [I>=2σ (I)]	R_1 = 0.0423, wR_2 = 0.1183
Final R indexes [all data]	R_1 = 0.0603, wR_2 = 0.1321
Largest diff. peak/hole / e Å^{-3}	0.17/-0.17
CCDC number	2089904

Table S20. Fractional Atomic Coordinates (×10^4) and Equivalent Isotropic Displacement Parameters (Å^2×10^3) for **1e·H_2O**. U_{eq} is defined as 1/3 of of the trace of the orthogonalised U_{IJ} tensor.

Atom	***x***	***y***	***z***	**U(eq)**
C1	3092(3)	1407(8)	3523(3)	48.6(12)
C3	3623(3)	126(7)	4975(3)	40.5(11)
C5	3816(3)	3665(7)	4618(3)	47.3(12)
C2	3200(3)	-187(7)	4110(3)	48.5(12)
C4	3931(3)	2106(7)	5234(3)	46.5(12)
C6	4103(3)	-1232(7)	6427(3)	67.2(15)
O2	3711(2)	-1531(5)	5519(2)	60.3(10)
O1	3338(2)	4856(5)	3176(2)	64.9(11)
N1	3419(2)	3332(6)	3770(3)	46.4(10)
O3	5000	6748(10)	2500	98(2)

Table S21. Anisotropic Displacement Parameters ($Å^2×10^3$) for **1e·H_2O**. The Anisotropic displacement factor exponent takes the form: $-2π^2[h^2a^{*2}U_{11}+2hka^*b^*U_{12}+…]$.

Atom	U_{11}	U_{22}	U_{33}	U_{23}	U_{13}	U_{12}
C1	44(3)	56(4)	45(3)	-8(3)	5(2)	-3(3)
C3	32(2)	42(3)	48(3)	3(3)	8(2)	-1(2)
C5	41(3)	45(3)	53(3)	-14(3)	0(2)	-3(2)
C2	46(3)	45(3)	54(3)	-7(3)	7(2)	-11(2)
C4	42(3)	49(4)	45(3)	1(3)	0.8(19)	1(2)
C6	61(3)	78(4)	63(3)	19(3)	9(3)	7(3)
O2	70(2)	51(2)	59(2)	13.0(18)	6.9(16)	-6.7(16)
O1	68(2)	59(2)	65(2)	19.9(18)	5.3(17)	5.1(16)
N1	36(2)	47(3)	56(3)	3(2)	8.7(18)	4.3(19)
O3	91(5)	64(4)	147(6)	0	42(4)	0

Table S22. Bond Lengths for **1e·H_2O**.

Atom	Atom	Length/Å	Atom	Atom	Length/Å
C1	C2	1.338(7)	C5	C4	1.348(7)
C1	N1	1.349(7)	C5	N1	1.291(7)
C3	C2	1.322(7)	C6	O2	1.369(7)
C3	C4	1.379(7)	O1	N1	1.312(5)
C3	O2	1.331(6)			

Table S23. Bond Angles for **1e·H_2O**.

Atom	Atom	Atom	Angle/˚	Atom	Atom	Atom	Angle/˚
C2	C1	N1	122.7(5)	C5	C4	C3	120.8(4)
C2	C3	C4	117.9(4)	C3	O2	C6	117.2(4)
C2	C3	O2	116.1(4)	C5	N1	C1	118.5(4)
O2	C3	C4	126.0(4)	C5	N1	O1	119.8(4)
N1	C5	C4	120.7(4)	O1	N1	C1	121.7(4)
C3	C2	C1	119.3(4)				

Table S24. Hydrogen Atom Coordinates ($Å×10^4$) and Isotropic Displacement Parameters ($Å^2×10^3$) for **1e·H_2O**.

Atom	*x*	*y*	*z*	U(eq)
H1	2778.61	1177.83	2919.38	58
H5	4024.34	4993.19	4805.09	57
H2	2979.47	-1500.51	3911.17	58
H4	4221.92	2370.71	5840.5	56
H6A	4140.65	-2533.95	6744.09	101
H6B	3678.18	-302.37	6692.38	101

Atom	*x*	*y*	*z*	U(eq)
H6C	4765.07	-648.41	6483.14	101
H3	4580(50)	6060(90)	2700(40)	120(20)

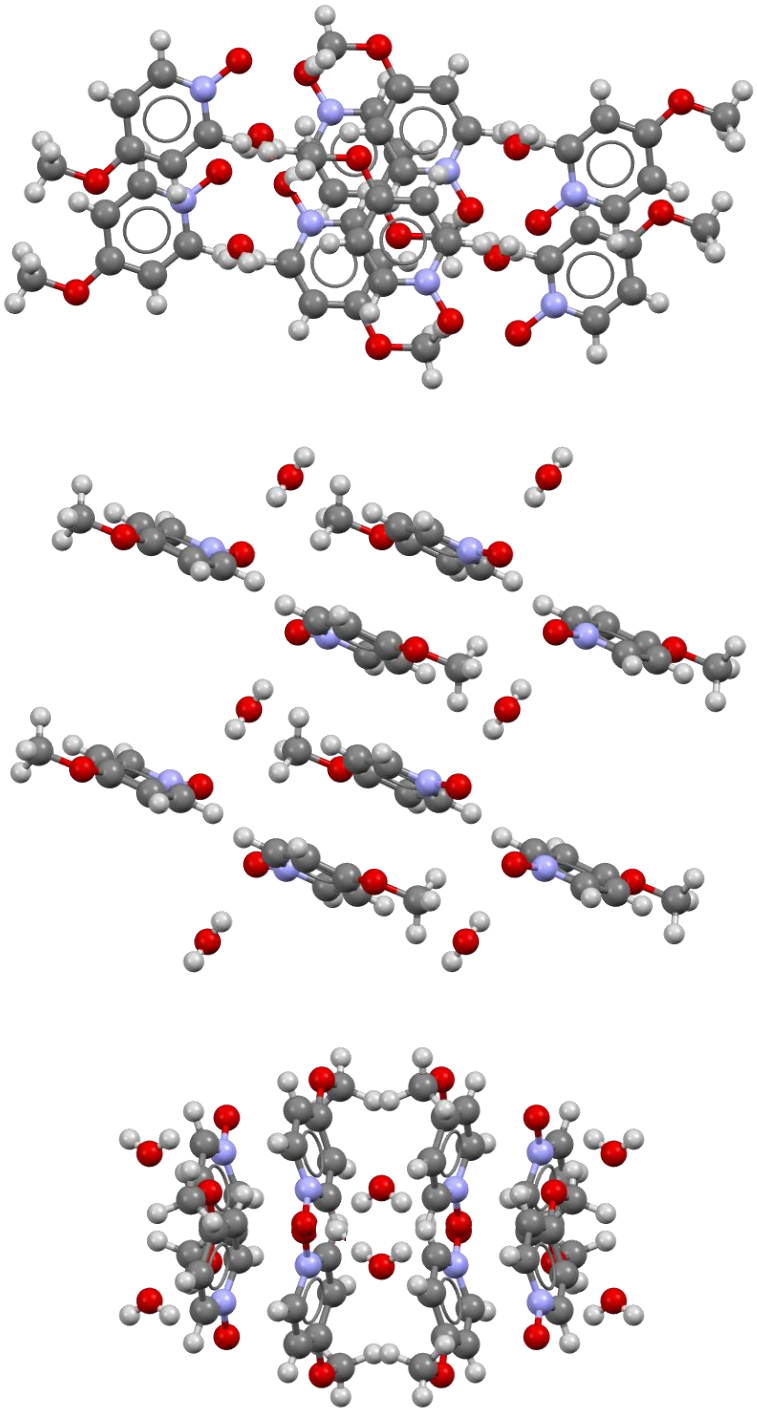

Figure S21. Packing of structure **1e·H_2O** from *a* axis (top), *b* axis (mid), *c* axis (bottom).

S4. CSD Surveys.

Table S25. Refcodes of structures present on the Cambridge Structural Database (CSD) containing OsO_4. Structures where a nucleophile (Nu) is engaging in a close contact with the osmium atom are in bold. The CSD search was made assuming that the Nu may be N, P, O, S, Se, F, Cl, Br, I.

CAHTAI T. Hasell, M. Schmidtmann, A. I. Cooper, *J. Am. Chem. Soc.* **2011**, *133*, 14920. DOI: 10.1021/ja205969q.

COTTEK R. Weber, K. Dehnicke, U. Muller, D. Fenske, *Z. Anorg. Allg. Chem.* **1984**, *516*, 214. DOI: 10.1002/zaac.19845160927.

NOLTIR A. J. Bailey, M. G. Bhowon, W. P. Griffith, A. G. F. Shoair, A. J. P. White, D. J. Williams, *J. Chem. Soc., Dalton Trans.* **1997**, 3245. DOI:10.1039/a702965i.

NOLTOX A. J. Bailey, M. G. Bhowon, W. P. Griffith, A. G. F. Shoair, A. J. P. White, D. J. Williams, *J. Chem. Soc., Dalton Trans.* **1997**, 3245. DOI:10.1039/a702965i.

QUIOSO W. P. Griffith, A. C. Skapski, K. A. Woode, M. J. Wright, *Inorg. Chim. Acta* **1978**, *31*, L413. DOI:10.1016/S0020-1693(00)94942-9.

RICTOM D. W. Nelson, A. Gypser, P. T. Ho, H. C. Kolb, T. Kondo, H.-L. Kwong, D. V. McGrath, A. E. Rubin, P.-O.Norrby, K. P. Gable, K. B. Sharpless, *J.Am.Chem.Soc.* **1997**, *119*, 1840. DOI: 10.1021/ja961464t.

RICTUS D. W. Nelson, A. Gypser, P. T. Ho, H. C. Kolb, T. Kondo, H.-L. Kwong, D. V. McGrath, A. E. Rubin, P.-O.Norrby, K. P. Gable, K. B. Sharpless, *J.Am.Chem.Soc.* **1997**, *119*, 1840. DOI: 10.1021/ja961464t.

RICVAA D. W. Nelson, A. Gypser, P. T. Ho, H. C. Kolb, T. Kondo, H.-L. Kwong, D. V. McGrath, A. E. Rubin, P.-O.Norrby, K. P. Gable, K. B. Sharpless, *J.Am.Chem.Soc.* **1997**, *119*, 1840. DOI: 10.1021/ja961464t.

SARDUK J.S.Svendsen, I.Marko, E.N.Jacobsen, C.P.Rao, S.Bott, K.B.Sharpless, *J.Org.Chem.* (1989), **54**, 2263. DOI: 10.1021/jo00271a002.

SUKJOX E. J. Corey, M. C. Noe, S. Sarshar, *J. Am. Chem. Soc.* **1993**, *115*, 3828. DOI: 10.1021/ja00062a080.

SUKJOX01 R. E. Marsh, *Acta Crystallogr., Sect. B: Struct. Sci.* **1999**, *55*, 931. DOI: 10.1107/S0108768199009441.

TIXXAZ E. J. Corey, S. Sarshar, M. D. Azimioara, R. C. Newbold, M. C. Noe, *J. Am. Chem. Soc.* **1996**, *118*, 7851. DOI: 10.1021/ja960536d.

ZATKEK W. P. Griffith, T. Y. Koh, A. J. P. White, D. J. Williams, *Polyhedron* **1995**, *14*, 2019. DOI: 10.1016/0277-5387(95)00041-P.

S5. Computational data.

S5.1 Theoretical methods

The energetic features of the adducts analyzed in this work were calculated at the PBE0[16]-D3[17]/def2-TZVP[18] level of theory using the crystallographic coordinates for the X-ray adducts and fully optimizations for the complexes in Figure 3 (see Main Text). For osmium, the inner shell electrons are modelled by ECPs (ECP-60 scheme),[19] which also accounts for scalar relativistic effects. The GAUSSIAN-16 program has been used for the energetic calculations and NBO analysis.[20] The basis set superposition error for the calculation of interaction energies has been corrected using the counterpoise method.[21] Molecular electrostatic potential (MEP) surfaces have been computed at the same level of theory and represented using several isovalues of electron density to map the electrostatic potential. The QTAIM analysis[22] has been performed using the AIMAll program[23] at the same level of theory.

The topological properties of electron density were analysed using the QTAIM methodology. A brief review of some relevant concepts within Bader's topology analysis is appropriate to facilitate the analysis of the results. The existence of a bond path linking two nuclei implies that the two atoms are bonded to one another. Such a path is characterized by the bond critical point, which is the point of minimum charge density along the bond, but a maximum along the directions perpendicular to the bond path. A critical point can be characterized by the number of zero eigenvalues of the associated Hessian matrix, which determines its rank, and the algebraic sum of their signs, which determine its signature. A bond critical point is denoted as (3,–1) and has one positive (λ_3) and two negative (λ_1, λ_2) curvatures, one (λ_3) associated with the charge density along the bond path and the other (λ_1, λ_2) perpendicular to the bond path. There can be other types of nondegenerate critical points: (3,–3), (3, +1), and (3, +3). The first corresponds to position of local maxima of the charge density (the nuclei). The two other types occur as a consequence of particular geometrical arrangements of bond paths and define elements of molecular structure. If the bond paths are linked so as to form a ring of bonded atoms, a (3, +1) ring critical bond is formed in the interior of the ring. If the bond paths are arranged as to enclose the interior of a molecule with ring surfaces, then a (3, +3) cage critical point is found in the interior of the cage, the charge density being a local minimum at such a point. The characteristics of the bond critical point (BCP) were discussed in terms of the electron density (ρ) and it's Laplacian ($\nabla^2\rho$).

The NCIplot[24,25] index allows convenient visualization of both inter and intra molecular interactions in real space. It plots isosurfaces of the reduced-density gradient (related to $|\nabla|/\rho^{4/3}$). The isosurfaces are coloured in agreement to values of the electron density. The NCI contacts are identified by the regions of small reduced density gradient (RDG) at low densities. These regions are mapped in real-space by plotting an isosurface of *s* for a low value of RDG. Besides, the sign of the second eigenvalue of the density Hessian times the density, is color-mapped onto the isosurfaces, which allows the characterization of both the strength and (un)favorable nature of these interactions. More precisely, the colour scheme is composed by a red–yellow–green–blue scale using red for repulsive (ρ^+_{cut}) and blue for attractive (ρ^-_{cut}) NCI interaction density. Weak repulsive and weak attractive interactions are identified by yellow and green surfaces, respectively.

The bonding analysis performed using EDA is based on the Morokuma, Ziegler, and Rauk scheme[26,27] focuses on the interaction energy ΔE_{int} of a bond A–B between two fragments A and B in a particular electronic reference state and in the frozen geometry AB. To do so, the optimized molecule is fragmented and single points are preset to obtain the electronic energy and the wave function. In a second step, the wave functions of the two fragments are combined to form the final molecular wave function and energy. This energy is divided into four main components: (1) electrostatic interaction ($\Delta E_{elestat}$), (2) Pauli repulsion (ΔE_{Pauli}), and (3) orbital interaction (ΔE_{orb}) and (4) Dispersion energy (E_{disp}). The term $\Delta E_{elestat}$ corresponds to the classical electrostatic interaction between the unperturbed charge distributions of the fragments. The Pauli repulsion (ΔE_{Pauli}) is the energy change associated with the transformation from the superposition of the unperturbed wave

functions of the isolated fragments to the final supramolecular wave function, which properly obeys the Pauli principle. It comprises the destabilizing interactions between electrons of the same spin on either fragment. The orbital interaction ΔE_{orb} accounts for charge transfer and polarization effects.[28] and ΔE_{disp} for dispersion effects. Further details on the EDA method can be found in the literature.[29]

EDA computations were done via the Perdew–Burke–Ernzerhof (PBE) exchange–correlation functional[30] with considering the empirical DFT-D3 scheme, implemented in the Amsterdam density functional (ADF) package.[31] For all atoms a triple-ξ STO basis set with two sets of polarization functions (TZ2P) was used. It was combined by zero order regular approximation (ZORA) to describe the relativistic effects in the heavier atoms (Ru and Os).

S5.2 IR results

Figure S22 shows the IR spectra of the isolated monomers OsO_4 and pyridine as well as of the adduct OsO_4···Py. It can be observed that the band at 975 cm^{-1} in pure OsO_4 is at 940 cm^{-1} in the adduct, that is in reasonable agreement with experiment taking into consideration that the calculations are in the gas phase and for the isolated adduct. The red-shift upon complexation is a bit underestimated compared to the experiment, partially due to the scale factor used for representing the IR spectra. The blue-shift of the pyridine breathing vibrations bands is also reproduced by theory. Finally, the blue-shift displacement of vC–H bands of pyridine rings and their decreased intensity upon complexation is also observed in the theoretical IR spectrum (see Figure 22c).

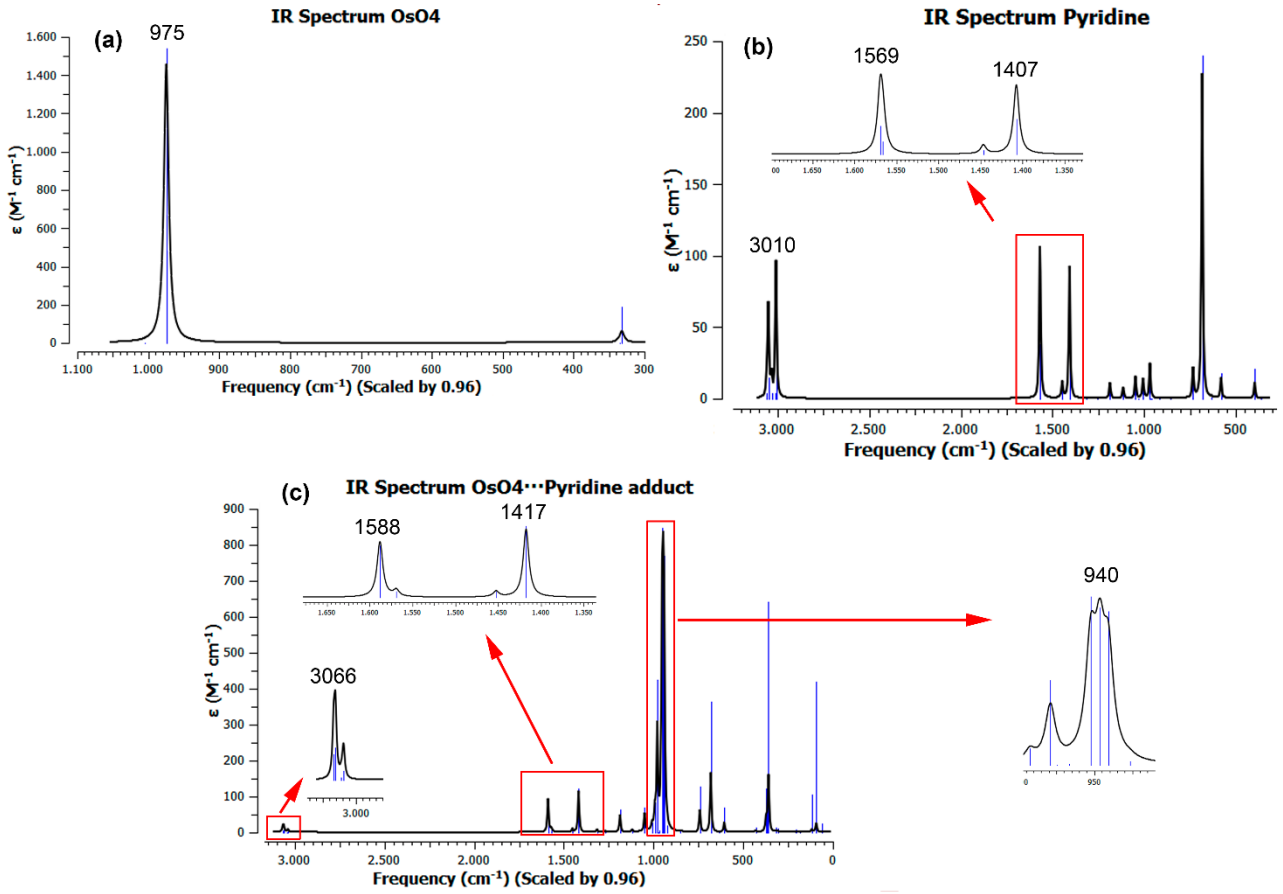

Figure S22. IR spectra of OsO_4 (a), pyridine (b) and the OsO_4···Py (c) at the PBE0-D3/def2-TZVP level of theory. The IR bands have been scaled by a factor of 0.96 as recommended by the National Institute of Standards and Technology (NIST) for this level of theory.[32]

S5.3 EDA analysis

As discussed above in S5.1, the computational tool of EDA decomposes the total binding energy of the adducts into four components :

$\Delta E_{total} = \Delta E_{Pauli} + \Delta E_{elestat} + \Delta E_{orb} + \Delta E_{disp}$

ΔE_{Pauli} represents the Pauli repulsion. $\Delta E_{elestat}$ is the classical electrostatic interaction energy, and ΔE_{orb} stands for the orbital energy including charge transfer and mixing terms. ΔE_{disp} refers to the dispersion term. The total binding energies and their components for the six dimers (Osme complexes) are listed in Table S26. An excellent correlation is found between the total binding energies in Table S26 and those in Table 1 ($R^2 = 0.997$), thus giving reliability to the EDA partition method (see Figure S23). It can be observed that the most favorable contribution is the electrostatic term in all complexes followed by dispersion in the $O_4Fe\cdots NCCH_3$, $O_4Fe\cdots NC_5H_5$ and $Ru\cdots NCCH_3$ complexes. For the rest of complexes, the orbital contribution is the second most important contribution, after electrostatic. This result that shows higher orbital contribution for the $RuO_4\cdots Py$ and $OsO_4\cdots Py$ complexes agrees well with the NBO analysis shown in Table 1 (see main text).

Table S26. The four components of the total binding energies obtained by the EDA scheme for the eight complexes (values are given in kcal/mol).

Compound	**ΔE_{Pauli}**	**$\Delta E_{elestat}$**	**ΔE_{orb}**	**ΔE_{disp}**	**ΔE_{total}**
$O_4Fe\cdots NCCH_3$	3.3	-2.89	-0.95	-1.83	-2.37
$O_4Fe\cdots NC_5H_5$	6.55	-5.97	-1.48	-3.61	-4.51
$O_4Ru\cdots NCCH_3$	5.68	-5.90	-1.61	-2.19	-4.02
$O_4Ru\cdots NC_5H_5$	35.55	-30.18	-10.93	-5.48	-11.04
$O_4Os\cdots NCCH_3$	8.53	-8.55	-2.65	-2.36	-5.03
$O_4Os\cdots NC_5H_5$	65.79	-54.12	-22.87	-6.72	-17.92

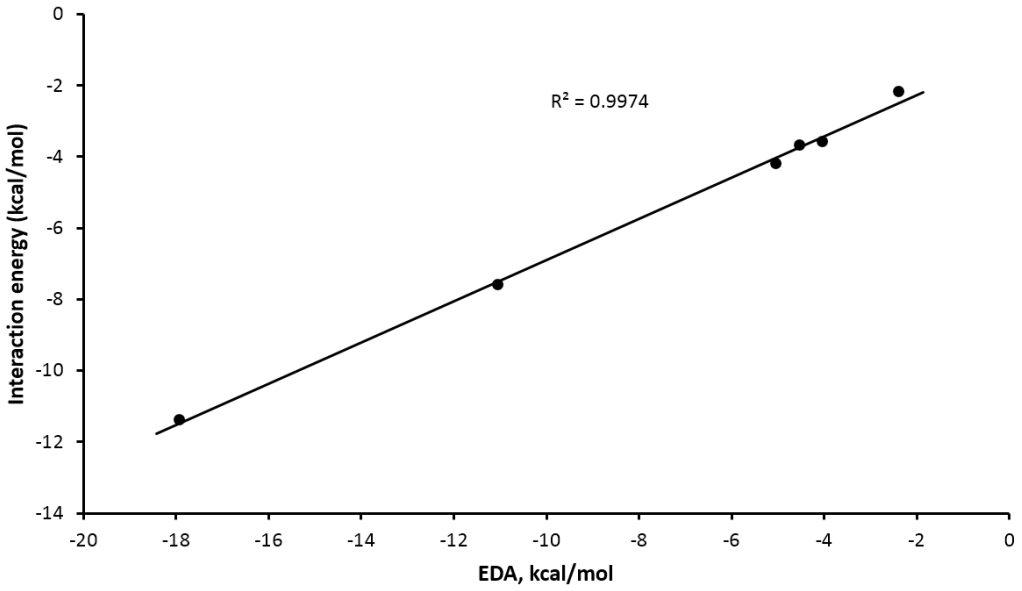

Figure S23. Regression plot of the interaction energies (Table 1, main text) vs the total EDA energies (ΔE_{total} values, Table S26).

S.5.4

Table S27. Osme interaction energies (E_{int}, kcal/mol) derived from the electron charge density (ρr), values at the bond CPs, distances (pm) between N/O and Om atoms, and ρ_r (a.u.) at the bond CPs connecting N/O and Om atoms for compounds **2a-c**.

Complex	E_{int}	Distance	ρ_r
2a	–14.5	239.4	0.0607
2b	–14.8	238.0	0.0627
2c	–14.7	230.5	0.0620

S5.5 Additional Theoretical Study of Os derivatives

Two $O_3Os{=}N\text{-}R$ imido structures (Refcodes ADOOSA and KEWMEE) and one $O_2Os(=N\text{-}R)_2$ diimido structure (Refcode ADOOSB) are present in the CSD. The MEP surfaces of these three compounds are shown in Figure S24. ADOOSA and KEWMEE have 3 identical σ-holes opposite to the Os-O bonds with energies of 15 and 18 kcal/mol, respectively and one less positive σ-hole opposite to the Os-N bond (+10 and +13 kcal/mol, respectively). The ADOOSB structure presents two identical σ-holes opposite to the Os-O bond (+3.4 kcal/mol) and two identical negative MEP values opposite to the Os-N bonds.

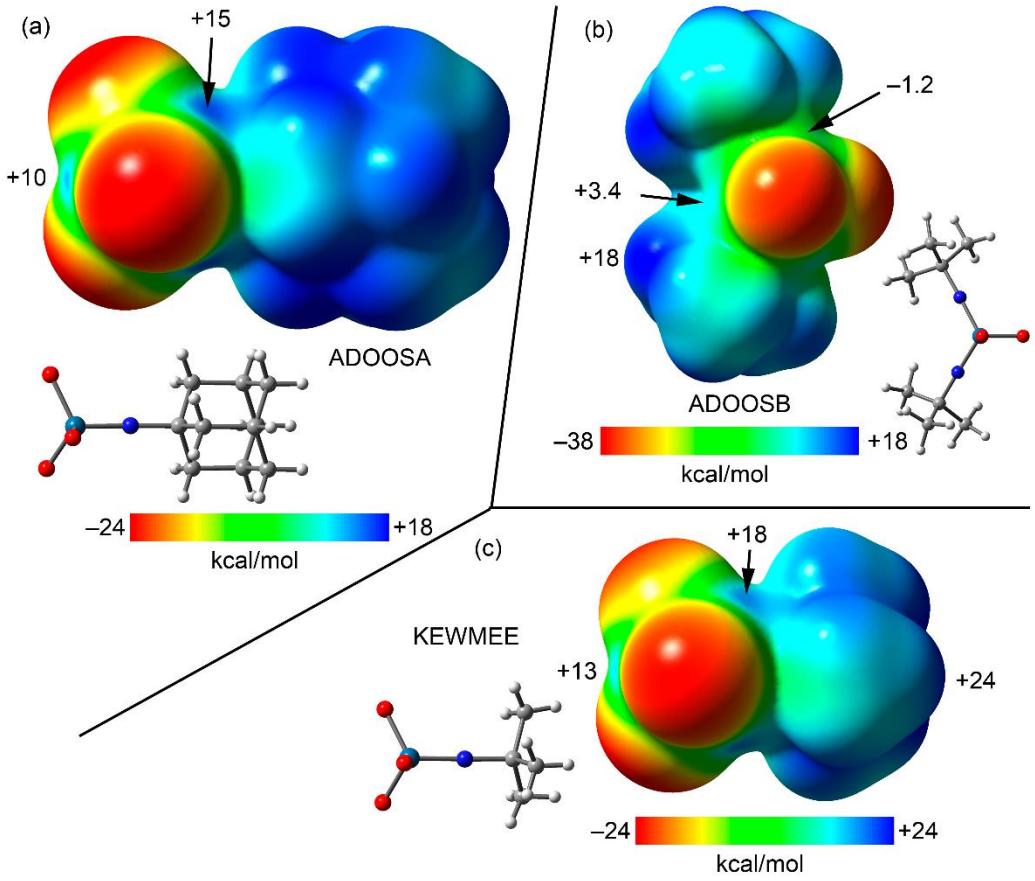

Figure S24. MEP surfaces of CSD structures ADOOSA (a) ADOOSB (b) and KEWMEE (c) at the PBE0-D3/def2-TZVP level of theory. The MEP values at selected points of the surfaces are given in kcal/mol

The MEP maxima in these compounds are nor located at osmium but at the aliphatic H-atoms (+18 kcal/mol in ADOOSA and ADOOSB and +24 kcal/mol in KEWMEE). Consistent with this feature, the solid state structure is basically governed by C–H···O contacts. Nonetheless, ADOOSA forms dimers in the solid state where two directional Os···O noncovalent interactions are established, with distances slightly above the sum of vdW radii (Figure S25). The NCIplot surface of the self-assembled dimers and its dimerization energy is shown in Figure S25. It can be observed an extended green (attractive) isosurface located between the two molecules, that embraces both the antiparallel Os–O bonds and the aliphatic H-atoms, thus evidencing the existence of both C–H···O and Os···O contacts. The value of the density at the surface measured at the crossing point of an hypothetical line connecting the interacting Os and O atoms is ρ = 0.0045 a.u., that is significantly smaller (one order of magnitude) than the values of ρ measured at the bond CPs that characterize the OmBs in the X-ray structures reported in this work (see Table S27), in line with the longer Os···O distances in the ADOOSA dimer. The existence of OmBs in this dimer evidences that OmBs are not limited to osmium tetroxide adducts.

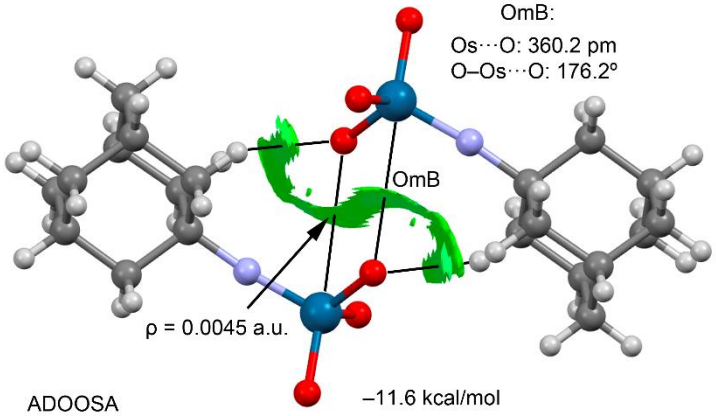

Figure 25. Self-assembled dimer observed in the X-ray structure of ADOOSA, NCIPlot: |RGB| isosurface 0.4 a.u.; Color range 0.03 a.u. ≤ (signλ_2)ρ ≤ –0.03 a.u. Only the intermolecular interactions are shown. The density value at the surface point between the Os and O atoms is given.

Finally, in order to further demonstrate that the osme bonding described in this work is different from that of a nucleophile with a positively charged metal center at high oxidation state, we analyzed the MEP surfaces of four additional model systems, *i.e.*, $OsO_{4-n}(=NCH_3)_n$ (n = 1-4). MEPs are represented in Figure S26 and values at σ-hole on osmium are reported in Table S28. Interestingly, σ-hole opposite to the $=NCH_3$ group progressively decreases from +16.3 kcal/mol in $OsO_3(=NCH_3)$ to –4.5 kcal/mol in $Os(=NCH_3)_4$, thus ruling out the simple nucleophile-charged metal explanation for the observed OmB interaction.

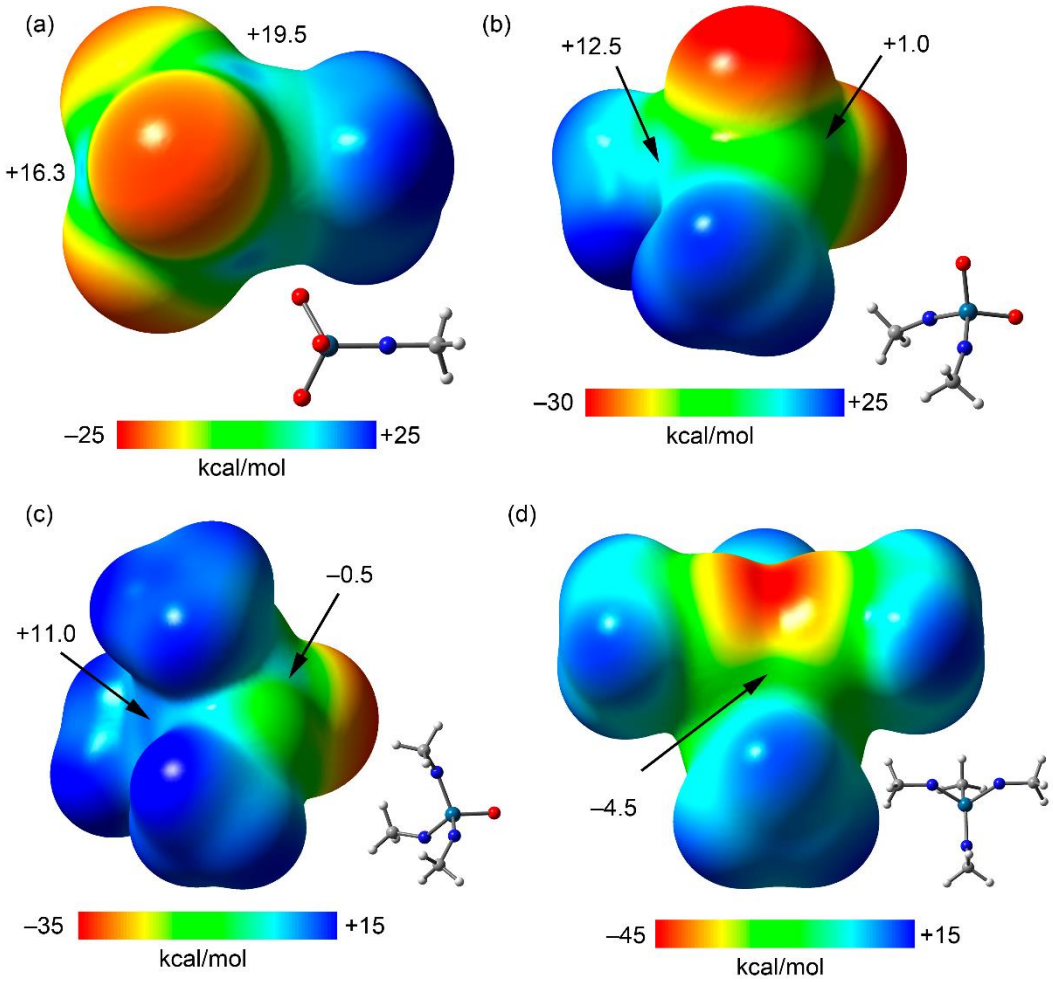

Figure S26. MEP surfaces of model compounds $OsO_{4-n}(=NCH_3)_n$ (n = 1-4) at the PBE0-D3/def2-TZVP level of theory.

Table S28. MEP values (kcal/mol) opposite to the Os=O and Os=N bonds in compounds $OsO_{4-n}(=NCH_3)_n$ (n = 1-4) at the PBE0-D3/def2-TZVP level of theory.

	$V_{s,O=Os}$	$V_{s,N=Os}$
$Os(=NCH_3)O_3$	19.5	16.3
$Os(=NCH_3)_2O_2$	12.5	1.0
$Os(=NCH_3)_3O$	11.0	–0.5
$Os(=NCH_3)_4$	-	–4.5

S5.6 CARTESIAN COORDINATES

$O_4Fe\cdots NCCH_3$

8	0.780801	-1.239925	-0.776666
8	0.818659	-0.038833	1.472691
8	2.887048	-0.047238	-0.003172
8	0.851208	1.307973	-0.692556
26	1.324840	-0.004162	0.000072
6	-3.228630	0.023265	-0.000418
7	-2.081017	0.072178	-0.001275
6	-4.676367	-0.038301	0.000707
1	-5.013514	-0.905002	0.571338
1	-5.088907	0.864713	0.453281
1	-5.048043	-0.122338	-1.021673

$O_4Fe\cdots NC_5H_5$

7	0.107946	1.312980	0.000000
6	1.338846	1.811240	0.000000
1	2.148943	1.085615	0.000000
6	1.613904	3.170998	0.000000
1	2.639742	3.521045	0.000000
6	0.549890	4.058753	0.000000
8	-1.652716	-1.289726	0.000000
8	0.549890	-1.529816	1.276914
6	-0.739227	3.549564	0.000000
1	-1.603350	4.203884	0.000000
6	-0.904854	2.172276	0.000000
1	-1.901096	1.736762	0.000000
8	-0.408543	-3.500632	0.000000
8	0.549890	-1.529816	-1.276914
1	0.722336	5.129118	0.000000
26	-0.239297	-1.947859	0.000000

$O_4Ru\cdots NCCH_3$

8	-0.520006	-0.369924	1.534970
8	-0.519461	-1.144249	-1.087781
8	-2.708110	-0.000205	-0.000320
8	-0.519881	1.514293	-0.446988
44	-1.041984	-0.000016	-0.000023
6	3.357546	0.000128	0.000178
7	2.209596	0.000378	0.000552
6	4.806059	-0.000196	-0.000287
1	5.179228	-1.007747	0.189339
1	5.179154	0.339122	-0.967776
1	5.179789	0.667786	0.777208

$O_4Ru\cdots NC_5H_5$

7	0.165369	1.259685	0.000000
6	1.408575	1.726598	0.000000
1	2.198627	0.981433	0.000000
6	1.700870	3.080350	0.000000

1	2.730762	3.415149	0.000000
6	0.648496	3.982697	0.000000
8	-1.754679	-0.751176	0.000000
8	0.648496	-1.104659	1.389053
6	-0.649070	3.497116	0.000000
1	-1.501150	4.165523	0.000000
6	-0.840957	2.124276	0.000000
1	-1.836608	1.690836	0.000000
8	-0.470548	-3.065646	0.000000
8	0.648496	-1.104659	-1.389053
1	0.837789	5.050141	0.000000
44	-0.222014	-1.417681	0.000000

$O_4Os\cdots NCCH_3$

8	-0.976541	-1.281547	-0.237662
8	1.596613	-0.208030	-0.246189
8	-0.000648	-0.017659	-2.455910
8	-0.619678	1.483594	-0.257377
6	0.000375	0.025984	3.524918
7	0.000670	0.017008	2.377527
6	0.000009	0.037288	4.973028
1	0.483601	-0.863883	5.352963
1	0.541028	0.911122	5.339129
1	-1.024915	0.073348	5.345258
76	-0.000062	-0.005660	-0.764350

$O_4Os\cdots NC_5H_5$

76	-0.096163	1.061652	0.000000
7	0.175689	-1.437002	0.000000
6	-0.926313	-2.181030	0.000000
1	-1.866546	-1.640193	0.000000
6	-0.888598	-3.563418	0.000000
1	-1.810814	-4.130526	0.000000
6	0.346966	-4.192418	0.000000
8	1.594486	0.854483	0.000000
8	-0.888598	0.574819	1.423439
6	1.493247	-3.415325	0.000000
1	2.479008	-3.863049	0.000000
6	1.360029	-2.036511	0.000000
1	2.220894	-1.376705	0.000000
8	-0.276056	2.744686	0.000000
8	-0.888598	0.574819	-1.423439
1	0.414164	-5.274282	0.000000

S6. References.

[1] Hayat, M. A. Principles and Techniques of Electron Microscopy: Biological Applications. Cambridge University Press. (2000) pp. 45–61. ISBN 0-521-63287-0.
[2] G. M. Sheldrick, *Acta Crystallogr. Sect. A Found. Adv.* **2015**, *71*, 3−8.
[3] G. M. Sheldrick, *Acta Crystallogr. Sect. C Struct. Chem.* **2015**, *71*, 3−8.
[4] A. L. Spek, *Acta Crystallogr. Sect. D Biol. Crystallogr.* **2009**, *65*, 148−155.
[5] P. Scilabra, G. Terraneo, A. Daolio, A. Baggioli, A. Famulari, C. Leroy, D. L. Bryce, G. Resnati, *Cryst. Growth Des.* **2020**, *20*, 916−922.
[6] A. Bondi, *J. Phys. Chem.* **1964**, *68*, 441–451.
[7] S. S. Batsanov, *Inorg. Materials* **2001**, *37*, 871–885.
[8] N. G. Row, R. Parthasarathy, *J. Am. Chem. Soc.* **1981**, *103*, 477–479.
[9] N. Ramasubbu, R. Parthasarathy, *Phosphorus Sulfur* **1987**, *31*, 221–229.
[10] T. S. C. Nyburg, C. H. Faerman, *Acta Cryst.* **1985**, *B41*, 274-279.
[12] S. Ikuta, *J. Mol. Struct. (Theochem)* **1990**, *205*, 191–201.
[13] S. L. Price, A. J. Stone, J. Lucas, F. S. Rowland, A. E.; Thornley, *J. Am. Chem. Soc.* **1994**, *116*, 4910–4918.
[14] S. S. Batsanov, *Struct. Chem.* **2000**, *11*, 177–183.
[15] N. L. Allinger, X. Zhoua, J. Bergsma, *J. Mol. Struct. (Theochem)* **1994**, *312*, 69–83.
[16] C. Adamo, V. Barone, *J. Chem. Phys.* **1999**, *110*, 6158−6170.
[17] F. Weigend, *Phys. Chem. Chem. Phys.* **2006**, *8*, 1057−1065.
[18] S. Grimme, J. Antony, S. Ehrlich, H. Krieg, *J. Chem. Phys.* **2010**, *132*, 154104.
[19] D. Andrae, U. Haeussermann, M. Dolg, H. Stoll and H. Preuss, *Theor. Chim. Acta* **1990**, *77*, 123−141.
[20] M. J. Frisch, G. W. Trucks, H. B. Schlegel, G. E. Scuseria, M. A. Robb, J. R. Cheeseman, G. Scalmani, V. Barone, G. A. Petersson, H. Nakatsuji, X. Li, M. Caricato, A. V. Marenich, J. Bloino, B. G. Janesko, R. Gomperts, B. Mennucci, H. P. Hratchian, J. V. Ortiz, A. F. Izmaylov, J. L. Sonnenberg, Williams, F. Ding, F. Lipparini, F. Egidi, J. Goings, B. Peng, A. Petrone, T. Henderson, D. Ranasinghe, V. G. Zakrzewski, J. Gao, N. Rega, G. Zheng, W. Liang, M. Hada, M. Ehara, K. Toyota, R. Fukuda, J. Hasegawa, M. Ishida, T. Nakajima, Y. Honda, O. Kitao, H. Nakai, T. Vreven, K. Throssell, J. A. Montgomery Jr., J. E. Peralta, F. Ogliaro, M. J. Bearpark, J. J. Heyd, E. N. Brothers, K. N. Kudin, V. N. Staroverov, T. A. Keith, R. Kobayashi, J. Normand, K. Raghavachari, A. P. Rendell, J. C. Burant, S. S. Iyengar, J. Tomasi, M. Cossi, J. M. Millam, M. Klene, C. Adamo, R. Cammi, J. W. Ochterski, R. L. Martin, K. Morokuma, O. Farkas, J. B. Foresman, D. J. Fox, Wallingford, CT, **2016**.
[21] S. F. Boys, F. Bernardi, *Mol. Phys.* **1970**, *19*, 553−566.
[22] R. F. W. Bader, *Chem. Rev.* **1991**, *91*, 893−928.
[23] T. A. Keith, TK Gristmill Software, OverlandPark KS, USA **2019**.
[24] E. R. Johnson, S. Keinan, P. Mori-Sánchez, J. Contreras-García, A. J. Cohen, W. Yang, *J. Am. Chem. Soc.* **2010**, *132*, 6498-6506.
[24] J. Contreras-García, E. R. Johnson, S. Keinan, R. Chaudret, J.-P. Piquemal, D. N. Beratan, W. Yang, *J. Chem. Theory Comput.* **2011**, *7*, 625-632.
[26] T. Ziegler, A. Rauk, *Inorg. Chem*., **1979**, *18*, 1755–1759.
[27] K. Morokuma, *J. Chem. Phys*., **1971**, 55, 1236–1244.
[28] F. M. Bickelhaupt, N. M. M. Nibbering, E. M. Van Wezenbeek, E. J. Baerends, *J. Phys. Chem.* **1992**, *96*, 4864–4873
[29] L. Zhao, S. Pan, N. Holzmann, P. Schwerdtfeger, G. Frenking, *Chem. Rev*. *2019*, *119*, 8781–8845.
[30] J. P. Perdew, K. Burke, M. Ernzerhof, Phys. Rev. Lett. 1996, 77, 3865–3868.
[31] G. te Velde, F. M. Bickelhaupt, E. J. Baerends, C. Fonseca Guerra, S. J. A. van Gisbergen, J. G. Snijders, T. Ziegler, *J. Comput. Chem*. 2001, 22, 931–967.

[32] https://cccbdb.nist.gov/vibscalejust.asp, accessed 06.07.2021